

NASA TECHNICAL NOTE



NASA TN D-8361 *c.1*

NASA TN D-8361

LOAN COPY: RE  
AFWL TECHNICAL  
HIRTLAND AFB



TECH LIBRARY KAFB, NM

EFFECTS OF WING LEADING-EDGE RADIUS  
AND REYNOLDS NUMBER ON LONGITUDINAL  
AERODYNAMIC CHARACTERISTICS  
OF HIGHLY SWEEP WING-BODY  
CONFIGURATIONS AT SUBSONIC SPEEDS

*William P. Henderson*  
*Langley Research Center*  
*Hampton, Va. 23665*





0134113

1. Report No. NASA TN D-8361	2. Government Accession No.	3. Recipient's Catalog No.
4. Title and Subtitle EFFECTS OF WING LEADING-EDGE RADIUS AND REYNOLDS NUMBER ON LONGITUDINAL AERODYNAMIC CHARACTERISTICS OF HIGHLY SWEEP WING-BODY CONFIGURATIONS AT SUBSONIC SPEEDS	7. Author(s) William P. Henderson	5. Report Date December 1976
		6. Performing Organization Code
9. Performing Organization Name and Address NASA Langley Research Center Hampton, VA 23665	12. Sponsoring Agency Name and Address National Aeronautics and Space Administration Washington, DC 20546	8. Performing Organization Report No. L-11017
		10. Work Unit No. 505-04-11-01
15. Supplementary Notes	16. Abstract <p>An investigation was conducted in the Langley low-turbulence pressure tunnel to determine the effects of wing leading-edge radius and Reynolds number on the longitudinal aerodynamic characteristics of a series of highly swept wing-body configurations. The tests were conducted at Mach numbers below 0.30, angles of attack up to <math>16^{\circ}</math>, and Reynolds numbers per meter from <math>6.57 \times 10^6</math> to <math>43.27 \times 10^6</math>. The wings under study in this investigation had leading-edge sweep angles of <math>61.7^{\circ}</math>, <math>64.61^{\circ}</math>, and <math>67.01^{\circ}</math> in combination with trailing-edge sweep angles of <math>0^{\circ}</math> and <math>40.6^{\circ}</math>. The leading-edge radii of each wing planform could be varied from sharp to nearly round.</p>	11. Contract or Grant No.
		13. Type of Report and Period Covered Technical Note
17. Key Words (Suggested by Author(s)) Reynolds number effects Aerodynamics Leading-edge radius effects	18. Distribution Statement Unclassified - Unlimited	14. Sponsoring Agency Code
19. Security Classif. (of this report) Unclassified	20. Security Classif. (of this page) Unclassified	21. No. of Pages 53
		22. Price* \$4.25
Subject Category 02		

EFFECTS OF WING LEADING-EDGE RADIUS AND REYNOLDS NUMBER ON  
LONGITUDINAL AERODYNAMIC CHARACTERISTICS OF HIGHLY SWEEP  
WING-BODY CONFIGURATIONS AT SUBSONIC SPEEDS

William P. Henderson  
Langley Research Center

SUMMARY

An investigation was conducted in the Langley low-turbulence pressure tunnel to determine the effects of wing leading-edge radius and Reynolds number on the longitudinal aerodynamic characteristics of a series of highly swept wing-body configurations. The tests were conducted at Mach numbers below 0.30, angles of attack up to  $16^{\circ}$ , and Reynolds numbers per meter from  $6.57 \times 10^6$  to  $43.27 \times 10^6$ . The wings under study in this investigation had leading-edge sweep angles of  $61.7^{\circ}$ ,  $64.61^{\circ}$ , and  $67.01^{\circ}$  in combination with trailing-edge sweep angles of  $0^{\circ}$  and  $40.6^{\circ}$ . The leading-edge radii of each wing planform could be varied from sharp to nearly round.

The results of this study indicate that for the sharp leading-edge wings, with a trailing-edge sweep angle of  $0^{\circ}$ , the experimental lift coefficient data are in excellent agreement with the theoretical estimates, potential flow plus leading-edge augmented vortex lift, over the test angle-of-attack range. Changing the wing leading-edge shape from a sharp to a finite radius has a significant effect on the aerodynamic characteristics of the wing-fuselage configuration. Because of the development of some leading-edge suction, the lift data lie between the potential and potential plus vortex estimates. The summation of the experimental leading-edge suction and vortex lift, for wings of the same sweep angle but differing leading-edge shapes, is the same even though the individual increments are a function of leading-edge shape. As the leading-edge sweep or the trailing-edge sweep was increased for the wings with finite leading-edge radii, the summation of the experimental leading-edge suction and vortex lift was greater than the theoretical estimate. Increasing Reynolds number, leading-edge radii, or trailing-edge sweep increased the angle of attack at which the experimental lift coefficient departed from the potential flow lift coefficient estimate.

INTRODUCTION

Aircraft of the future will probably be required to operate efficiently over a very large flight envelope. For example, aircraft designed for efficient supersonic cruise must

also be designed for efficient off-design performance. Off-design characteristics, such as take-off and landing requirements, subsonic cruise, and loiter characteristics, must be considered early in an aircraft design cycle so that the primary design goals can be achieved without adversely affecting the size or performance of the vehicle. The design principles associated with efficient supersonic design may not be compatible with either efficient subsonic and transonic cruise or maneuvering characteristics. As technology in aircraft design has developed, methods for improving multimission capability have been sought. One such method, the subject of this paper, designs the wings to achieve fully attached (potential) flow at the cruise and loiter conditions and controlled leading-edge separation (vortex flows) at maneuvering conditions. A significant amount of vortex lift is thereby achieved. There are, however, some indications that a wing designed to cruise with vortex lift present may be advantageous. With such a wing, the added lift results in a reduction in cruise angle of attack and, therefore, a reduction in cruise drag. Discussions of the principle of vortex lift are presented in references 1 and 2. Both attached (potential) flow at low angles of attack and full vortex flow at high angles of attack may be achieved by careful design of the wing leading-edge shape.

This paper presents an analysis of data obtained for a series of wings (leading-edge sweep between  $61.7^\circ$  and  $67.01^\circ$ ) covering planforms of interest in the design of supersonic cruise vehicles. Each wing concept was studied with several leading-edge shapes over a wide range of Reynolds numbers to determine the effect of these parameters on the longitudinal aerodynamic characteristics of the configuration.

This study was conducted in the Langley low-turbulence pressure tunnel at Mach numbers less than 0.30 and angles of attack from  $-5^\circ$  to  $16^\circ$ .

## SYMBOLS

The results given in this paper are referred to the stability axis system with the exception of the lift and drag coefficients, which are referred to the wind axis system. The force and moment data for each wing planform are nondimensionalized with respect to its own geometric characteristics (see fig. 1). The moment reference center was located at a point 59.00 cm rearward of the nose along the model reference line (see fig. 1).

$C_D$  drag coefficient,  $\frac{\text{Drag}}{q_\infty S_{\text{ref}}}$

$C_{D,0}$  drag at zero lift

$C_L$  lift coefficient,  $\frac{\text{Lift}}{q_\infty S_{\text{ref}}}$

$C_m$	pitching-moment coefficient, $\frac{\text{Pitching moment}}{q_\infty S_{\text{ref}} \bar{c}}$
$C_N$	normal-force coefficient, $\frac{\text{Normal force}}{q_\infty S_{\text{ref}}}$
$C_s$	leading-edge suction-force coefficient
$\bar{c}$	mean geometric chord, cm
$k_{\text{potential}}$	potential-lift factor (see ref. 2)
$k_{v,le}$	leading-edge vortex-lift factor (see ref. 2)
$q_\infty$	free-stream dynamic pressure
$R$	Reynolds number, per meter
$R_{\bar{c}}$	Reynolds number based on wing mean geometric chord
$S_{\text{ref}}$	wing reference area, m <sup>2</sup>
$\alpha$	angle of attack, deg
$\alpha_B$	angle at which lift coefficient departs from potential flow estimate, deg
$\Lambda_{le}$	wing leading-edge sweep angle, deg
$\Lambda_{te}$	wing trailing-edge sweep angle, deg

### MODEL DESCRIPTION

Geometric details of the model are presented in figure 1. The configuration had a midwing with zero dihedral and a cylindrical fuselage with an ogive nose. The wing was composed of a slab-shaped center section to which various leading-edge and trailing-edge extensions could be attached. The leading-edge extensions, representing leading-edge sweep angles of 61.7<sup>o</sup>, 64.61<sup>o</sup>, and 67.01<sup>o</sup>, were studied. For each leading-edge sweep,

a maximum of three leading-edge shapes were available for study: one shape had a sharp wedge section, and the other two shapes had rounded sections with average leading-edge radii (perpendicular to the wing leading edge) of 0.050 cm and 0.121 cm, respectively. For each leading-edge configuration, two trailing-edge extensions were available: one with a trailing-edge sweep angle of  $0^{\circ}$ , the second with a trailing-edge sweep angle of  $40.6^{\circ}$ .

### TESTS AND CORRECTIONS

Tests were conducted in the Langley low-turbulence pressure tunnel at Mach numbers below 0.30 and at angles of attack of up to  $16^{\circ}$ . The test Reynolds number per meter varied from  $6.57 \times 10^6$  to  $43.27 \times 10^6$ . Transition strips, 0.32 cm wide, of No. 150 carborundum grains were placed 1.00 cm behind the leading edge of the wings and 2.54 cm behind the nose of the fuselage. Corrections to the model angle of attack were made for deflections of the balance and sting support system under aerodynamic load. The lift coefficient and drag coefficient data were corrected for jet boundary and blockage effect. The drag data were adjusted to correspond to free-stream static conditions in the balance chamber. No attempt was made to correct data for any possible aeroelastic distortion caused by load at high dynamic pressures.

### PRESENTATION OF RESULTS

The basic data for each configuration studied are presented in figures 2 to 13 and are summarized in figures 14 to 18. As an aid in locating a particular part of the data, the following index of figures is presented.

	Figure
Effect of Reynolds number on longitudinal aerodynamic characteristics of configuration with –	
$\Lambda_{le} = 61.7^{\circ}$ , $\Lambda_{te} = 0^{\circ}$ , and sharp leading edge . . . . .	2
$\Lambda_{le} = 61.7^{\circ}$ , $\Lambda_{te} = 0^{\circ}$ , and small leading-edge radius . . . . .	3
$\Lambda_{le} = 61.7^{\circ}$ , $\Lambda_{te} = 0^{\circ}$ , and large leading-edge radius . . . . .	4
$\Lambda_{le} = 61.7^{\circ}$ , $\Lambda_{te} = 40.6^{\circ}$ , and sharp leading edge . . . . .	5
$\Lambda_{le} = 61.7^{\circ}$ , $\Lambda_{te} = 40.6^{\circ}$ , and large leading-edge radius . . . . .	6
$\Lambda_{le} = 64.61^{\circ}$ , $\Lambda_{te} = 0^{\circ}$ , and sharp leading edge . . . . .	7
$\Lambda_{le} = 64.61^{\circ}$ , $\Lambda_{te} = 0^{\circ}$ , and large leading-edge radius . . . . .	8
$\Lambda_{le} = 67.01^{\circ}$ , $\Lambda_{te} = 0^{\circ}$ , and sharp leading edge . . . . .	9
$\Lambda_{le} = 67.01^{\circ}$ , $\Lambda_{te} = 0^{\circ}$ , and small leading-edge radius . . . . .	10

	Figure
$\Lambda_{le} = 67.01^\circ$ , $\Lambda_{te} = 0^\circ$ , and large leading-edge radius . . . . .	11
$\Lambda_{le} = 67.01^\circ$ , $\Lambda_{te} = 40.6^\circ$ , and sharp leading edge . . . . .	12
$\Lambda_{le} = 67.01^\circ$ , $\Lambda_{te} = 40.6^\circ$ , and large leading-edge radius . . . . .	13
Effect of leading-edge profile on leading-edge vortex flow characteristics for configuration with leading-edge sweep of $61.7^\circ$ and trailing-edge sweep of $0^\circ$ . . . . .	14
Effect of leading-edge sweep on leading-edge vortex flow characteristics for configuration with trailing-edge sweep of $0^\circ$ . . . . .	15
Effect of trailing-edge sweep on leading-edge vortex flow characteristics for configuration with leading-edge sweep of $61.7^\circ$ and large leading-edge radius . . . . .	16
Effect of Reynolds number on leading-edge vortex flow characteristics for configuration with leading-edge sweep of $61.7^\circ$ , trailing-edge sweep of $0^\circ$ , and large leading-edge radius . . . . .	17
Effect of leading-edge radius and trailing-edge sweep on variation of angle of attack at which leading-edge separation starts as function of Reynolds number . . . . .	18

## RESULTS AND DISCUSSION

Since the drag data presented here have been previously analyzed and presented in the published literature (see ref. 3), only the general trends of the data are discussed in this paper, and the primary discussion considers only the lift and pitching-moment coefficient data. The lift and pitching-moment data on each figure are compared primarily with two theoretical estimates; one estimate is based on potential flow, and the other estimate is based on potential plus vortex flow. The potential flow estimate was made by using the method of reference 4, and the vortex flow estimate was made by using the method of reference 2. The estimated lift coefficients for potential flow presented in these figures do not include the contribution of the leading-edge suction to the lift. To illustrate the effect of this component on the lift, the leading-edge suction contribution to lift calculated by

$$k_{v,le} \cos \Lambda_{le} \sin^3 \alpha$$

is plotted in figures 3 and 11 at the lowest Reynolds number. As expected, these data indicated that the contribution of leading-edge suction to lift is very small for the wings of

this study at the test angle-of-attack range. The vortex-lift increment is the contribution of the leading edge and the augmented portions. The concept of augmented vortex lift was developed because for many delta wings the leading-edge vortex generated on the wing persists for a considerable distance downstream and, therefore, can act on other surfaces, such as the aft part of wing planforms. No contribution of the side edge was included because of the high taper ratio of the wing, which naturally results in very small wing tip chord for any direct generation of vortex lift. The experimental data are compared with the theoretical estimates in a limited number of cases to reduce the clutter in the figures.

The drag data for the wings with the sharp leading edges (see figs. 2, 5, 7, 9, and 12) agree very well with the theory for potential flow plus vortex flow over the entire test lift coefficient range investigated. These characteristics should be expected since sharp leading-edge wings do not develop any leading-edge suction. As either the leading-edge radius or Reynolds number is increased for wings with finite leading-edge radii, leading-edge suction is developed, and the data agree with the potential flow theory over a particular lift coefficient range which varies. As indicated in reference 3 and illustrated in these data (see fig. 8, for example), the lift coefficient at which the drag data depart from the potential flow theory is highly dependent on both Reynolds number and leading-edge radius. For all three sharp leading-edge wings with a trailing-edge sweep angle of  $0^\circ$  (see figs. 2, 7, and 9), the agreement of the experimental lift data with the potential flow plus vortex flow theory is excellent over the entire test angle-of-attack range. In this application of the vortex theory, only the leading edge and augmentation effects are accounted for. Therefore, the relative insignificance of the side effects for most of these highly tapered wings seems to be substantiated. The agreement between theoretical and experimental pitching-moment coefficient data is excellent in the low to intermediate lift coefficient range. At the higher lift coefficients, the configuration is less stable than the theory indicates, probably because of the nonlinear effects generated by the large fuselage nose at the higher lift coefficients.

As shown in figure 5, the agreement between theory (potential plus vortex) and experiment for the configuration with a wing leading-edge sweep of  $61.7^\circ$ , a trailing-edge sweep of  $40.6^\circ$ , and a sharp leading edge is excellent up to an angle of attack of about  $11^\circ$ . Above this angle of attack, the experimental lift falls significantly below the theory. As explained in reference 2 and demonstrated by the theoretical estimates, the leading-edge vortex generated on the wing can persist for a considerable distance downstream and, therefore, can act on other surfaces, such as the aft portion of a wing. Removal of the aft portion of the wing reduces the vortex-lift contribution (compare figs. 2 and 5) to the total lift. Since the theoretical reduction of augmented vortex lift is demonstrated by the theory, the lower value of the experimental lift with respect to the theory probably results from vortex breakdown. The data of figure 12, for a wing with the same trailing-edge sweep but a higher leading-edge sweep, do not exhibit this departure from the theory. This agreement is not

surprising since wing sweep is known to have an effect on the stability of the vortex system. (See ref. 5.)

Changing the wing leading-edge shape from a sharp to a finite radius is shown in this study to have a significant effect on the aerodynamic characteristics of the wing-fuselage configurations. (See fig. 4.) Two effects can be noted from the data presented in this study: first, the experimental lift no longer agrees with the full potential plus vortex flow estimate; second, the angle of attack at which the experimental lift coefficient data depart from the attached potential theory increases with increasing Reynolds number. For wings with finite leading-edge radii fully attached (potential), flow can be developed up to an angle of attack where leading-edge separation occurs and a leading-edge vortex is formed. This separation probably occurs first near the wing tip and moves inboard (see data of ref. 6) as the angle of attack is increased. In this case, part of the leading-edge thrust goes into vortex lift, and part remains as leading-edge suction. These results show clearly that a wing can be designed to develop full potential flow (for low drag) at cruise conditions and to develop vortex lift, for maneuver improvement, at higher angles of attack.

The effect of leading-edge radius on the vortex flow characteristics is summarized by the data presented in figure 14. On each chart, the experimental data are referenced to two theoretical estimates. The short-dashed line is the estimate for the full vortex normal-force increment for the leading edge only, and the long-dashed line is the estimate for the leading-edge plus augmented vortex lift. For differing leading-edge radii in all three cases, the sum of the experimental vortex normal-force increment is obtained by extraction from the experimental normal-force data

$$C_{N,vortex} = C_{N,experimental} - C_{N,potential}$$

when

$$C_{N,potential} = k_{potential} \sin \alpha \cos \alpha$$

and the experimental leading-edge suction is obtained by

$$C_s = \left[ C_L(\tan \alpha) - (C_D - C_{D,0}) \right] \sec \Lambda_{le} \cos \alpha$$

These sums add together algebraically to give the total available leading-edge suction (vortex normal-force increment). However, as the leading-edge radius is increased for a constant Reynolds number, less of the available leading-edge suction is actually turned into vortex lift. At low angles of attack, all the suction force on the wings with finite leading-edge radii is developed at the wing leading edge (experiment agrees with theory

for leading edge only). These results would be expected since the wing at these conditions exhibits attached flow. At the higher angles of attack, however, when leading-edge separation is initiated and vortex flow is formed, the sum of the experimental vortex lift and leading-edge suction agrees, as expected, with the theory for leading edge plus augmented vortex lift.

The effects of leading-edge sweep angle on the distribution of vortex normal force and leading-edge suction are illustrated in figure 15 for the configuration with a trailing-edge sweep of  $0^\circ$  and the large leading-edge radius. As the leading-edge sweep is increased, the magnitude of the leading-edge suction is reduced. This reduction is not surprising since this leading-edge suction comparison is made at a constant free-stream Reynolds number, and reference 3 indicates that the developed suction is a function of the Reynolds number, based on the component of flow perpendicular to the wing leading edge which naturally reduces as the wing sweep increases. The sum of the vortex normal force and leading-edge suction effects becomes larger than the full potential vortex estimate (leading edge plus augmented) at the higher leading-edge sweep angles. These results are not fully understood; however, they may be attributed to wing tip vortex effects (wing tip separation induced vortex) which have not been previously accounted for in the theoretical estimate. This conclusion is substantiated by the addition of the theoretical estimate for the full-potential vortex normal force (including leading-edge, augmented, and side-edge effects) to the comparison for the configuration with the leading-edge sweep of  $67.01^\circ$ . This estimate is in excellent agreement with the summation of the experimental leading-edge suction and vortex normal force.

The effect of trailing-edge sweep on the summation of the vortex normal force and leading-edge suction for the wing with a leading-edge sweep of  $61.7^\circ$  and large leading-edge radius is presented in figure 16. An interesting result is that a larger percentage of the available leading-edge effects remains as leading-edge suction and a smaller percentage goes into vortex normal force for the wing with the trailing-edge sweep of  $40.6^\circ$ . These results, as well as the indication of vortex breakdown on this wing, are probably tied to the distribution of the thrust along the wing leading edge. The wing with the trailing-edge sweep of  $40.6^\circ$  has a more constant variation of leading-edge suction (reduction of large peaks in suction) along the wing span than does the wing with the trailing-edge sweep of  $0^\circ$ . This type of distribution can undoubtedly help maintain attached flow on the wing. However, reference 2 illustrated that the more triangular leading-edge suction distribution is conducive to maintaining vortex stability once the leading-edge vortex is formed. These data also confirm the trend indicated by the vortex breakdown for the wing with the trailing-edge sweep of  $40.6^\circ$ . In addition, the summation of the vortex effects and the leading-edge suction is greater than the theoretical estimate (leading edge plus augmented). The determination of augmented effects, primarily through empirical approaches, may account for some of the disagreement. The data of reference 2 also indicated that as the taper ratio

is increased, the tip effects become more pronounced. Therefore, this disagreement may again be due to the lack of inclusion of tip effects (tip separation induced vortex).

The effect of Reynolds numbers on the distribution of the vortex normal force and leading-edge suction is presented in figure 17. As illustrated here and discussed in detail in reference 3, increasing Reynolds number reduces leading-edge separation and increases the developed leading-edge suction. These data at both Reynolds numbers again illustrate that while the distribution of suction and vortex normal force may vary, the total of both increments equals the full potential estimated vortex normal force.

Figure 18 illustrates the effect of Reynolds number (Reynolds number based on the component of velocity normal to the wing leading edge), leading-edge radius, and trailing-edge sweep angle on the angle of attack at which the experimental lift coefficient data depart from the potential flow estimated lift. The predominant effect seen in this figure is the large change in departure angle of attack with increasing Reynolds number. These results are primarily caused by the delay of leading-edge separation as Reynolds number is increased. There is also a significant increase in departure angle of attack with increased leading-edge radius because the leading-edge radius again delays leading-edge separation as Reynolds number is increased. As indicated previously, the spanwise distribution of leading-edge suction is somewhat flatter for the wing with the trailing-edge sweep angle of  $40.6^\circ$ . This distribution probably contributes to delayed leading-edge separation evidenced in figure 18.

## CONCLUSIONS

A wind-tunnel study has been conducted to determine the effects of wing leading-edge radius and Reynolds number on the longitudinal aerodynamic characteristics of a series of highly swept wing-body configurations at subsonic speeds. As a result of this study, the following conclusions can be made:

1. For the sharp leading-edge wings with a trailing-edge sweep angle of  $0^\circ$ , the experimental lift coefficient data are in excellent agreement with the estimated data (potential plus leading edge and augmented vortex lift) over the test angle-of-attack range.
2. Changing the wing leading-edge shape from a sharp to a finite radius has a significant effect on the aerodynamic characteristics of the wing-fuselage configuration. Because of the development of some leading-edge suction, the lift data lie between the potential and the potential plus vortex flow estimate.
3. The summation of the experimental leading-edge suction and vortex lift, for wings of the same sweep angle but differing leading-edge shapes, is the same even though the individual increments are a function of leading-edge shape.

4. As the leading-edge sweep or trailing-edge sweep was increased for the wings with finite leading-edge radii, the summation of the experimental leading-edge suction and vortex lift was greater than the theoretical estimate.

5. Increasing Reynolds number, leading-edge radii, or trailing-edge sweep increased the angle of attack at which the experimental lift coefficient departed from the potential flow lift coefficient estimate.

Langley Research Center  
National Aeronautics and Space Administration  
Hampton, VA 23665  
November 19, 1976

## REFERENCES

1. Polhamus, Edward C.: A Concept of the Vortex Lift of Sharp-Edge Delta Wings Based on a Leading-Edge-Suction Analogy. NASA TN D-3767, 1966.
2. Lamar, John E.: Some Recent Applications of the Suction Analogy to Vortex-Lift Estimates. Aerodynamic Analyses Requiring Advanced Computers, Part II, NASA SP-347, 1975, pp. 985-1011.
3. Henderson, William P.: Studies of Various Factors Affecting Drag Due to Lift at Subsonic Speeds. NASA TN D-3584, 1966.
4. Lamar, John E.: A Modified Multhopp Approach for Predicting Lifting Pressures and Camber Shape for Composite Planforms in Subsonic Flow. NASA TN D-4427, 1968.
5. Polhamus, Edward C.: Predictions of Vortex-Lift Characteristics by a Leading-Edge Suction Analogy. J. Aircr., vol. 8, no. 4, Apr. 1971, pp. 193-199.
6. Lamar, John E.; and McKinney, L. Wayne: Low-Speed Static Wind-Tunnel Investigation of a Half-Span Fuselage and Variable-Sweep Pressure Wing Model. NASA TN D-6215, 1971.

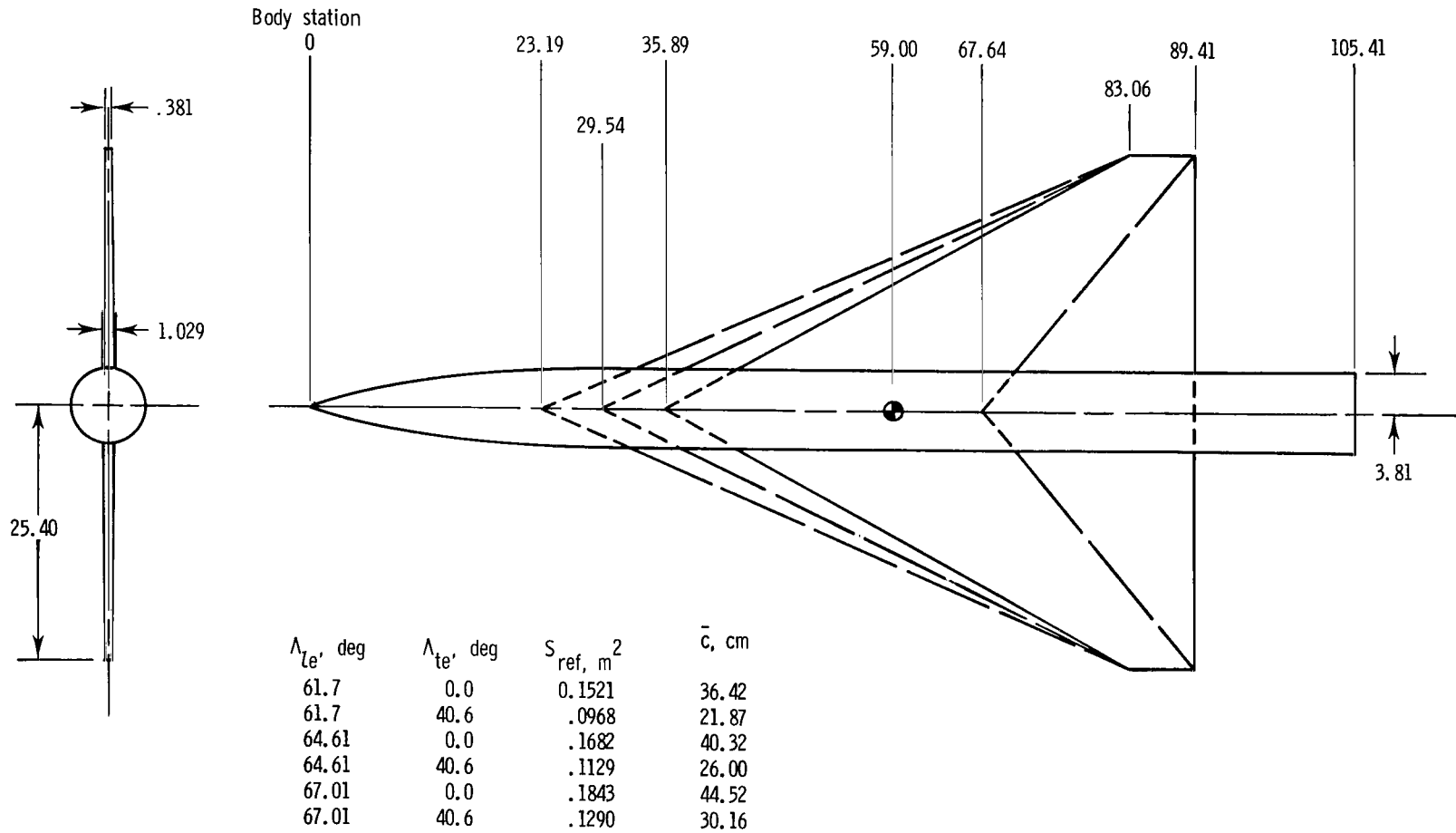


Figure 1.- Drawing of model showing wings studied in this investigation.

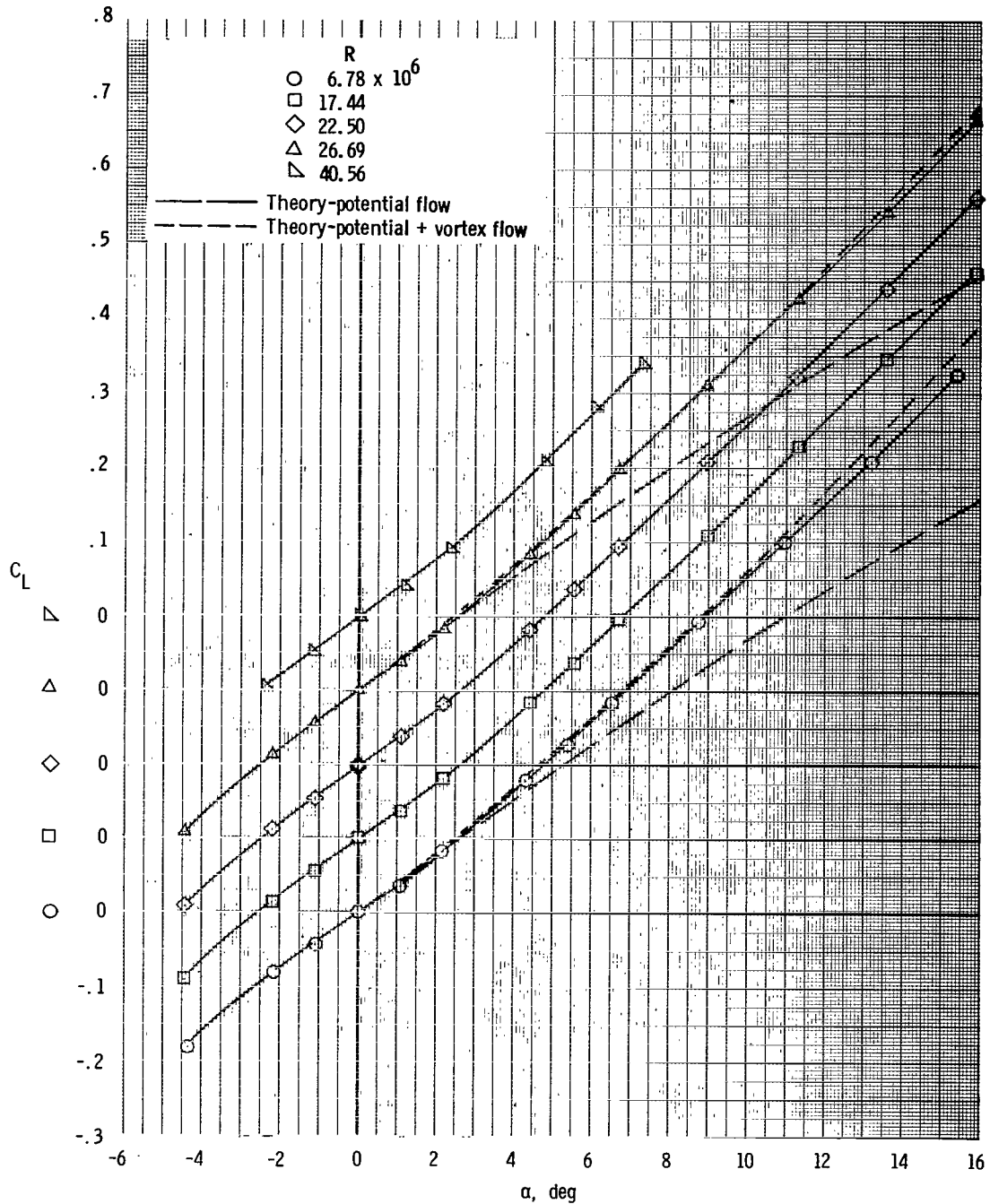


Figure 2.- Effect of Reynolds number on longitudinal aerodynamic characteristics of configuration with leading-edge sweep of  $61.7^\circ$ , trailing-edge sweep of  $0^\circ$ , and sharp leading edge.

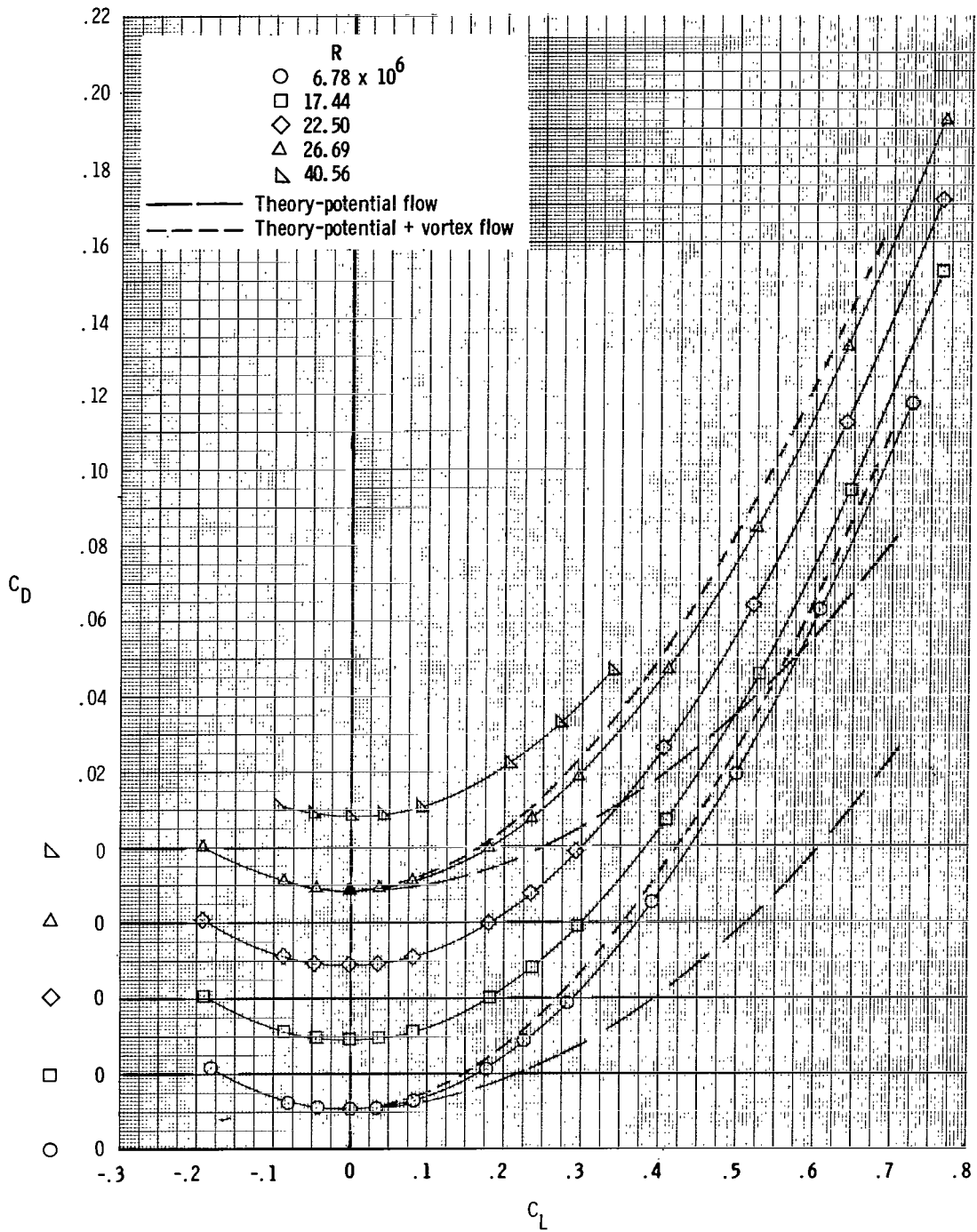


Figure 2.- Continued.

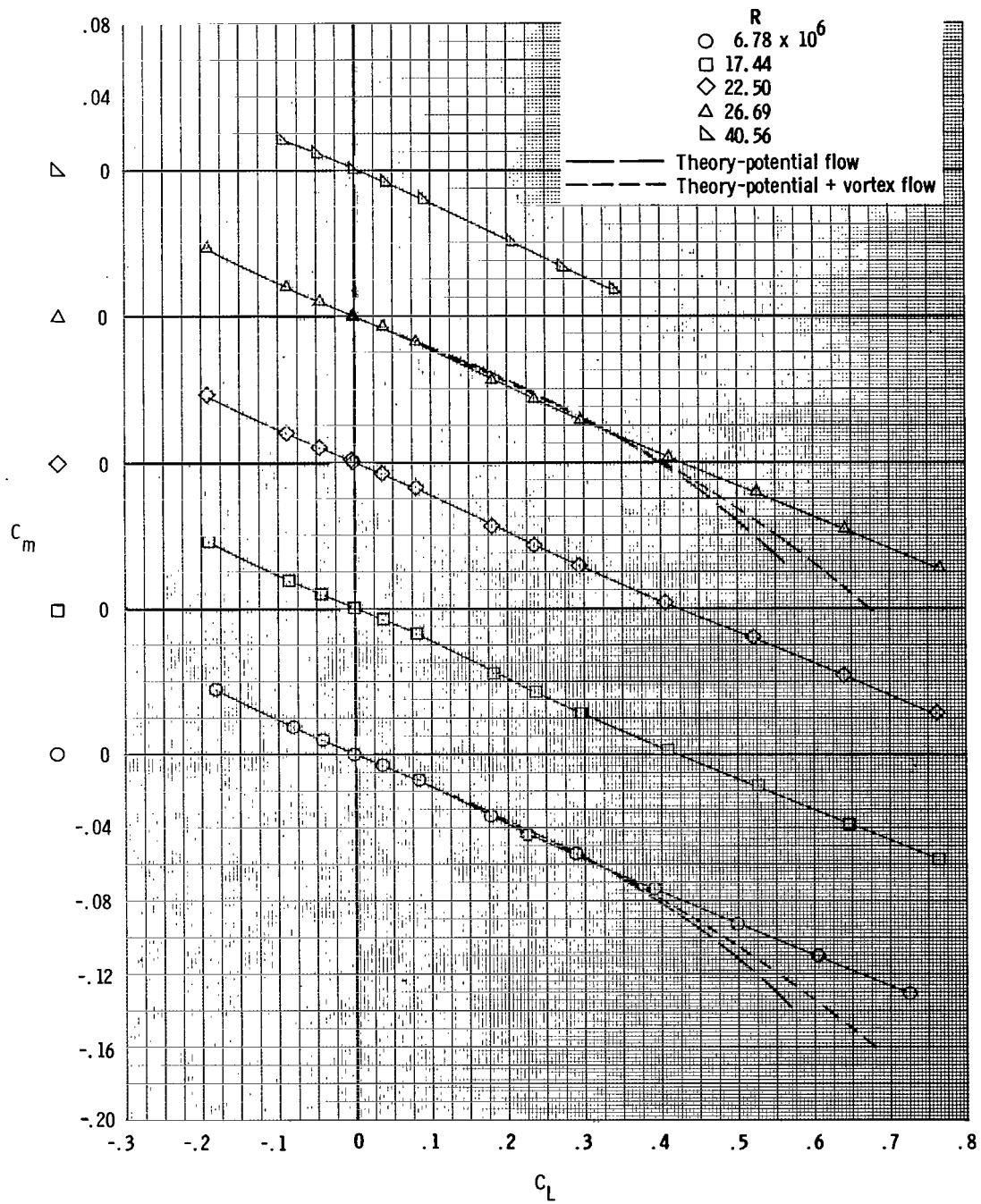


Figure 2.- Concluded.

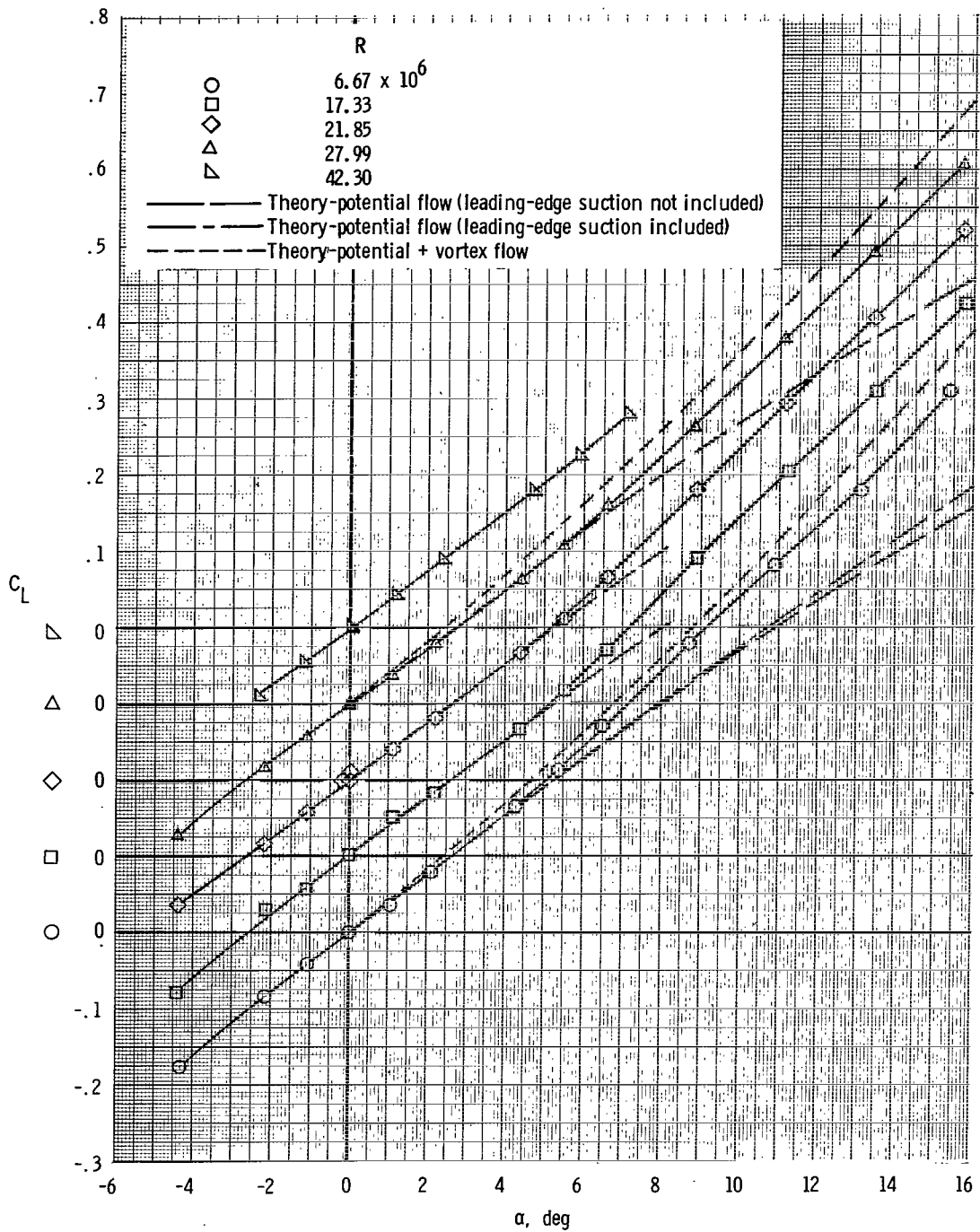


Figure 3.- Effect of Reynolds number on longitudinal aerodynamic characteristics of configuration with leading-edge sweep of  $61.7^\circ$ , trailing-edge sweep of  $0^\circ$ , and small leading-edge radius.

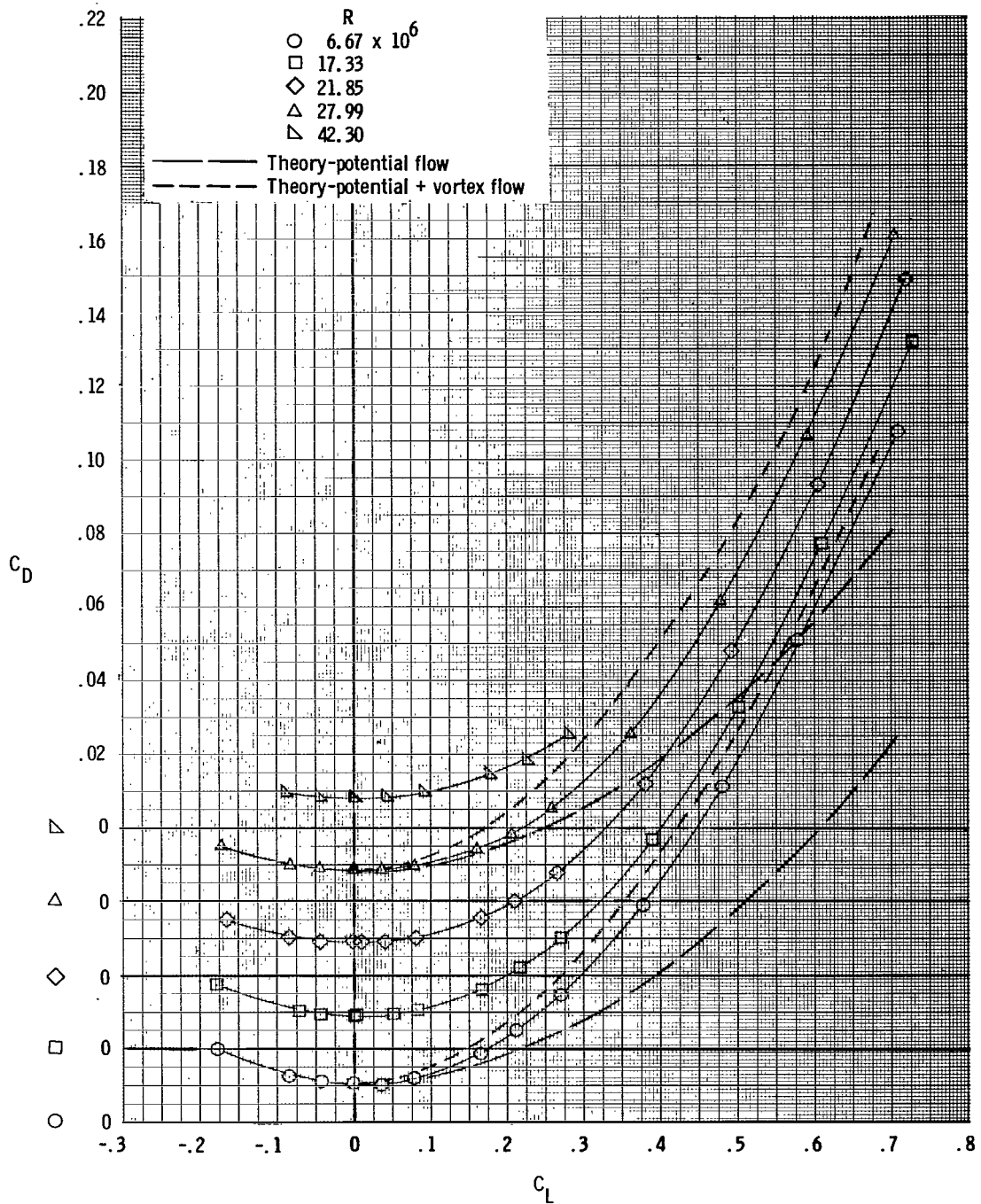


Figure 3.- Continued.



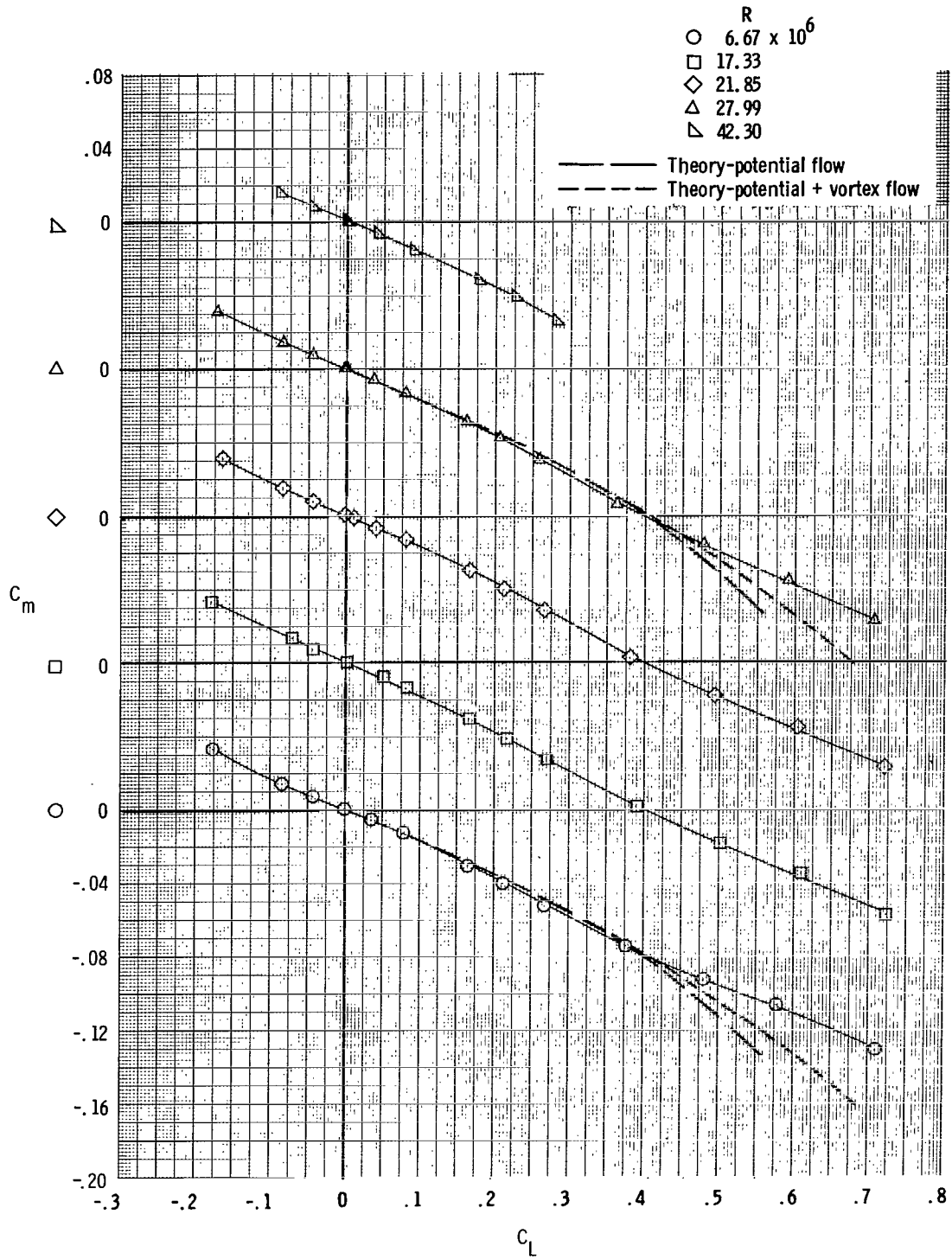


Figure 3.- Concluded.

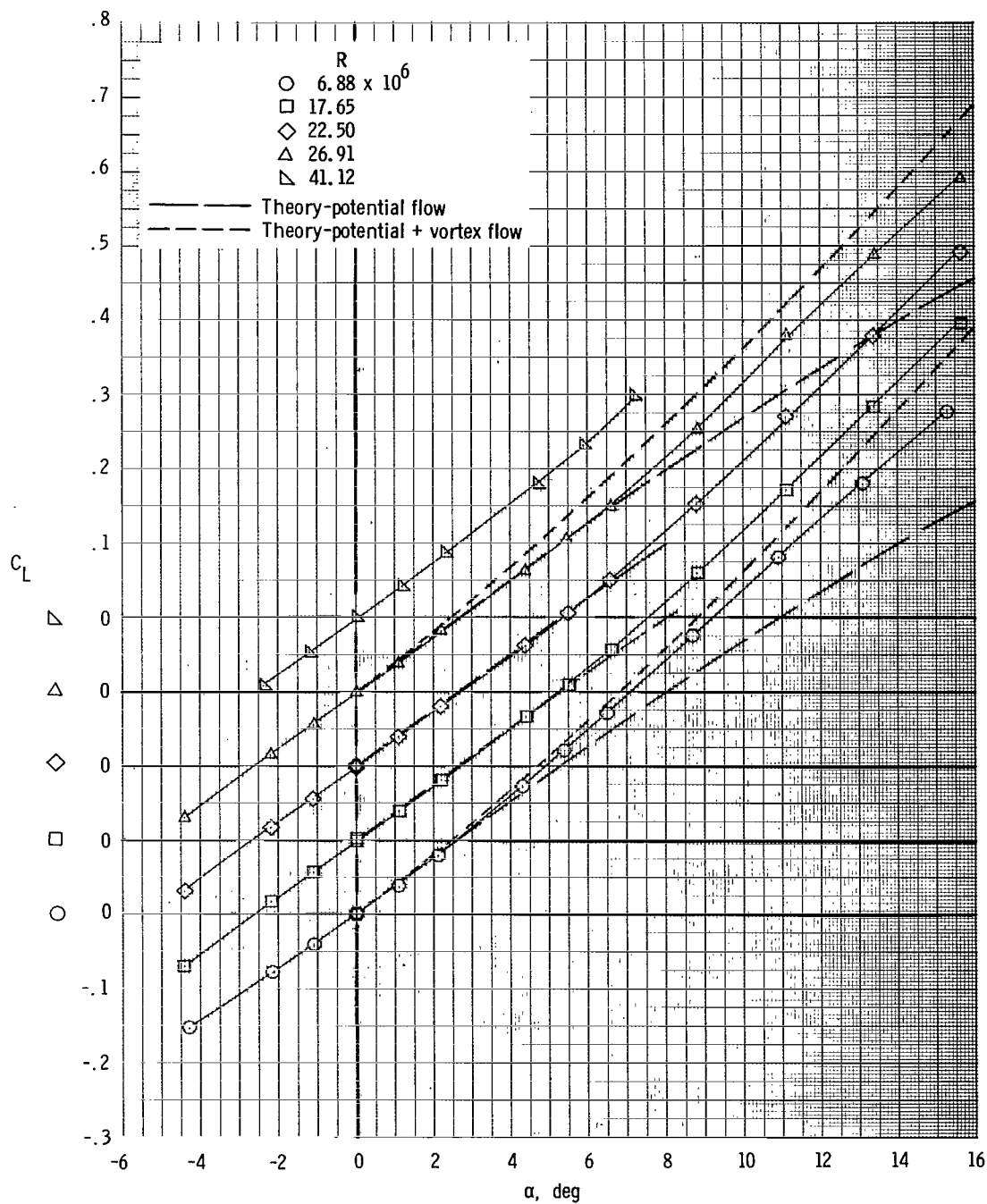


Figure 4.- Effect of Reynolds number on longitudinal aerodynamic characteristics of configuration with leading-edge sweep of  $61.7^\circ$ , trailing-edge sweep of  $0^\circ$ , and large leading-edge radius.

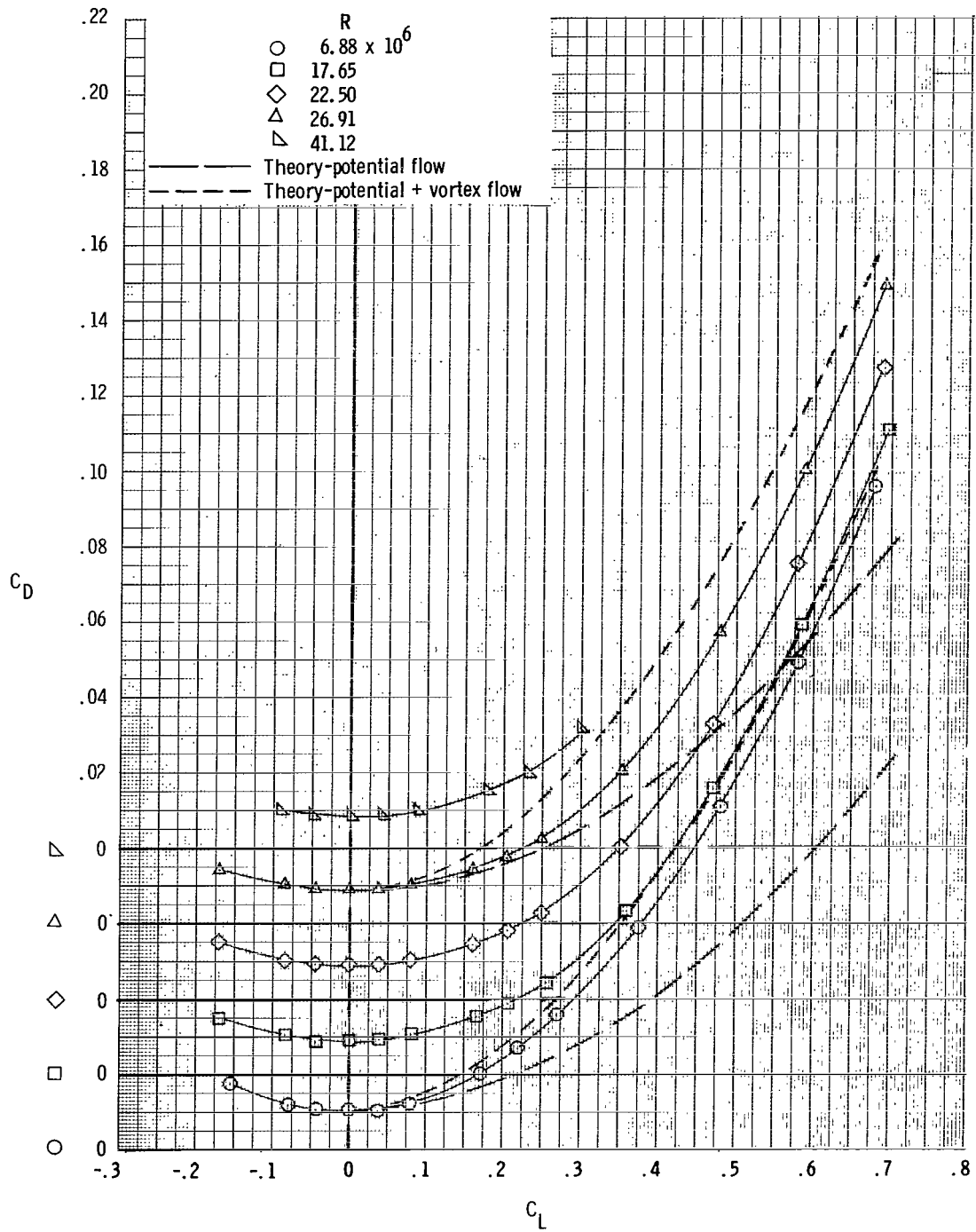


Figure 4.- Continued.

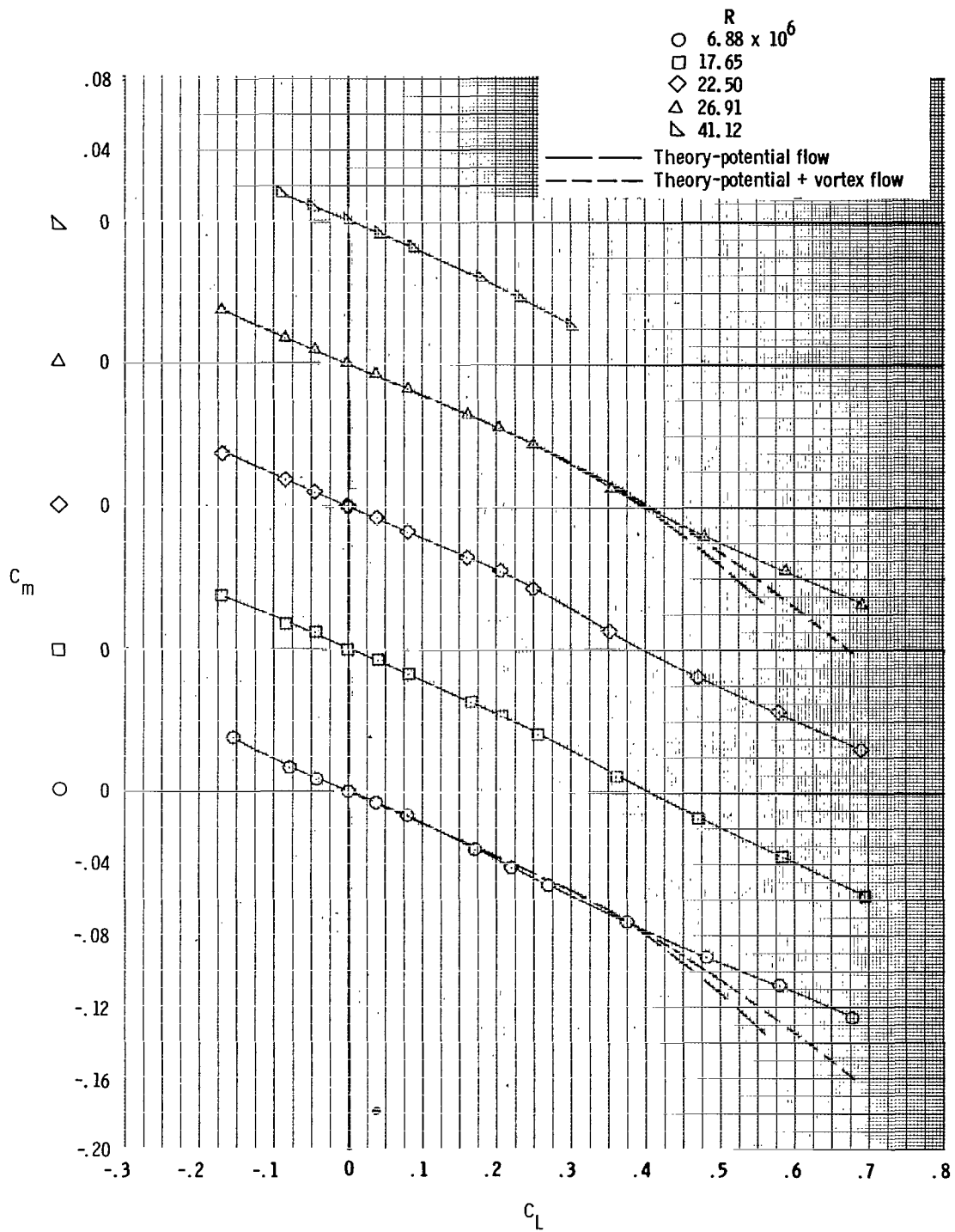


Figure 4.- Concluded.

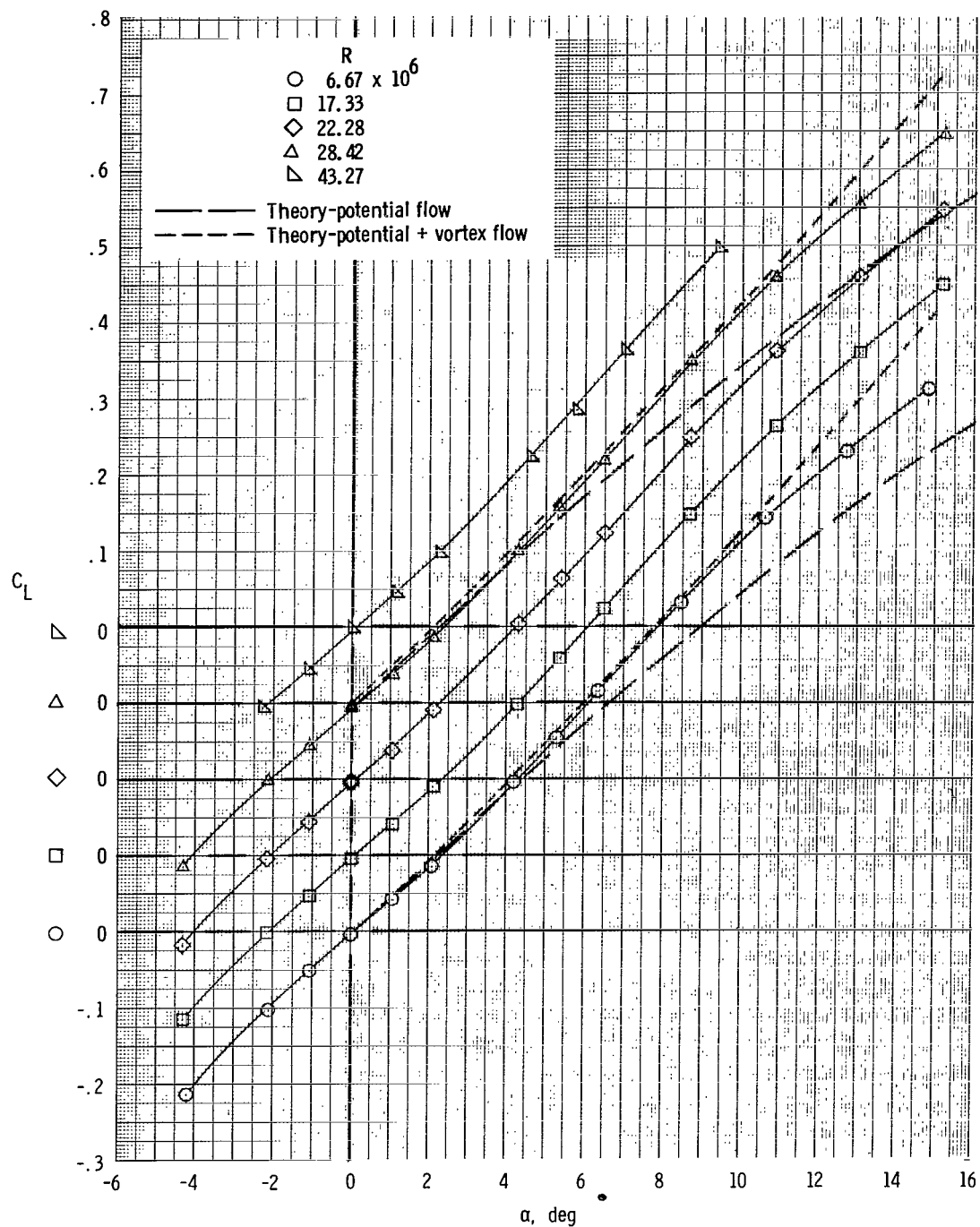


Figure 5.- Effect of Reynolds number on longitudinal aerodynamic characteristics of configuration with leading-edge sweep of  $61.7^\circ$ , trailing-edge sweep of  $40.6^\circ$ , and sharp leading edge.

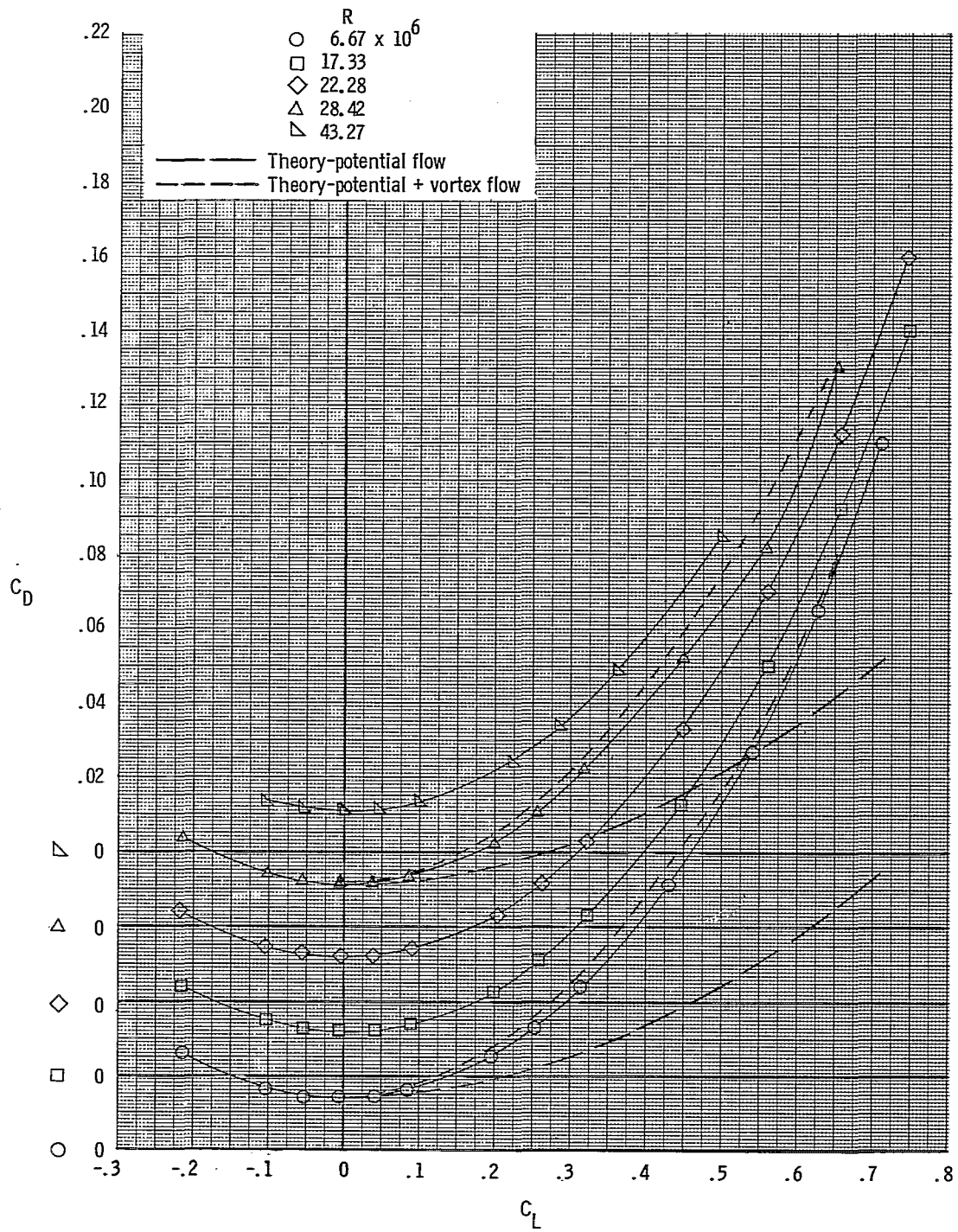


Figure 5.- Continued.

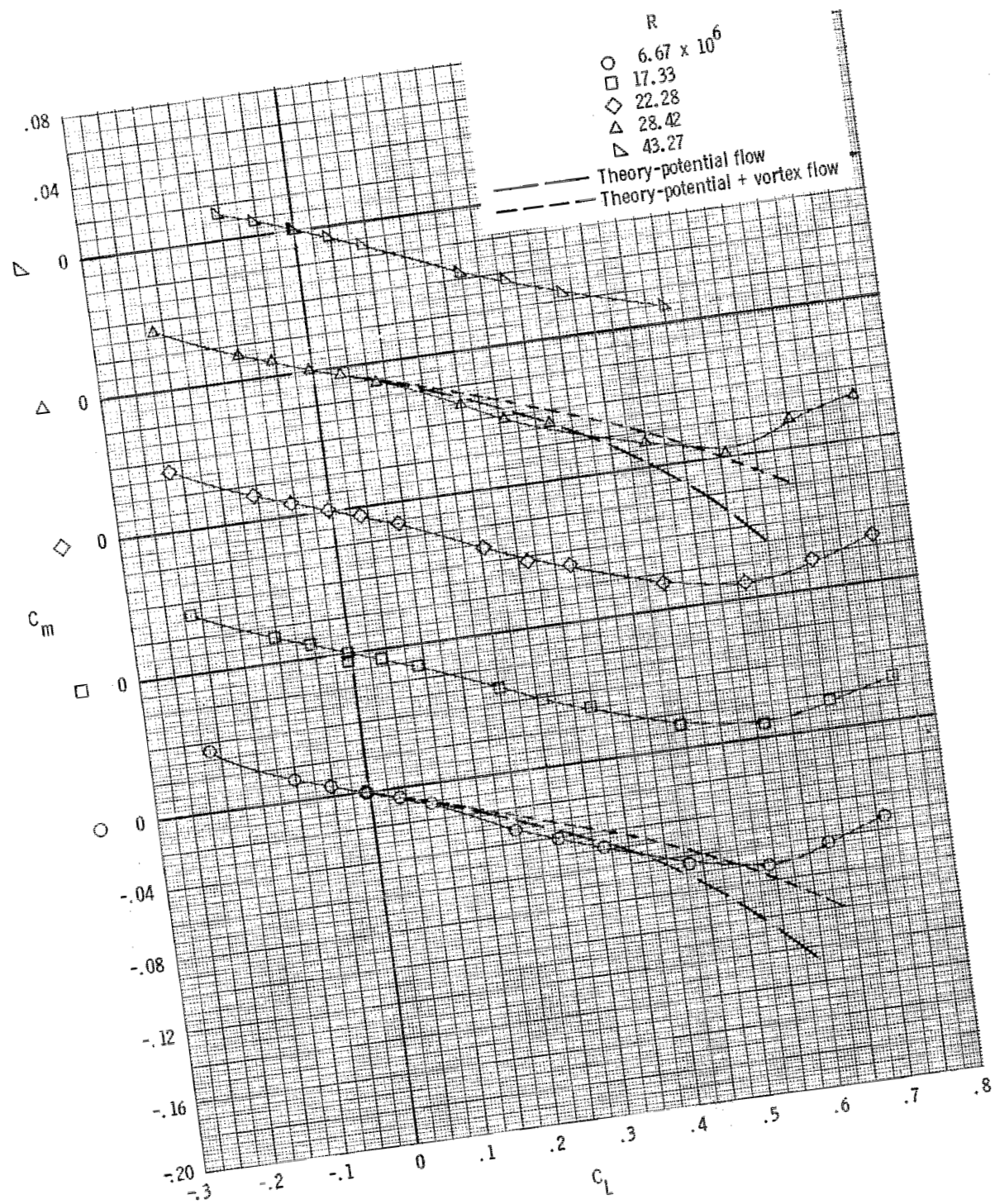


Figure 5.- Concluded.

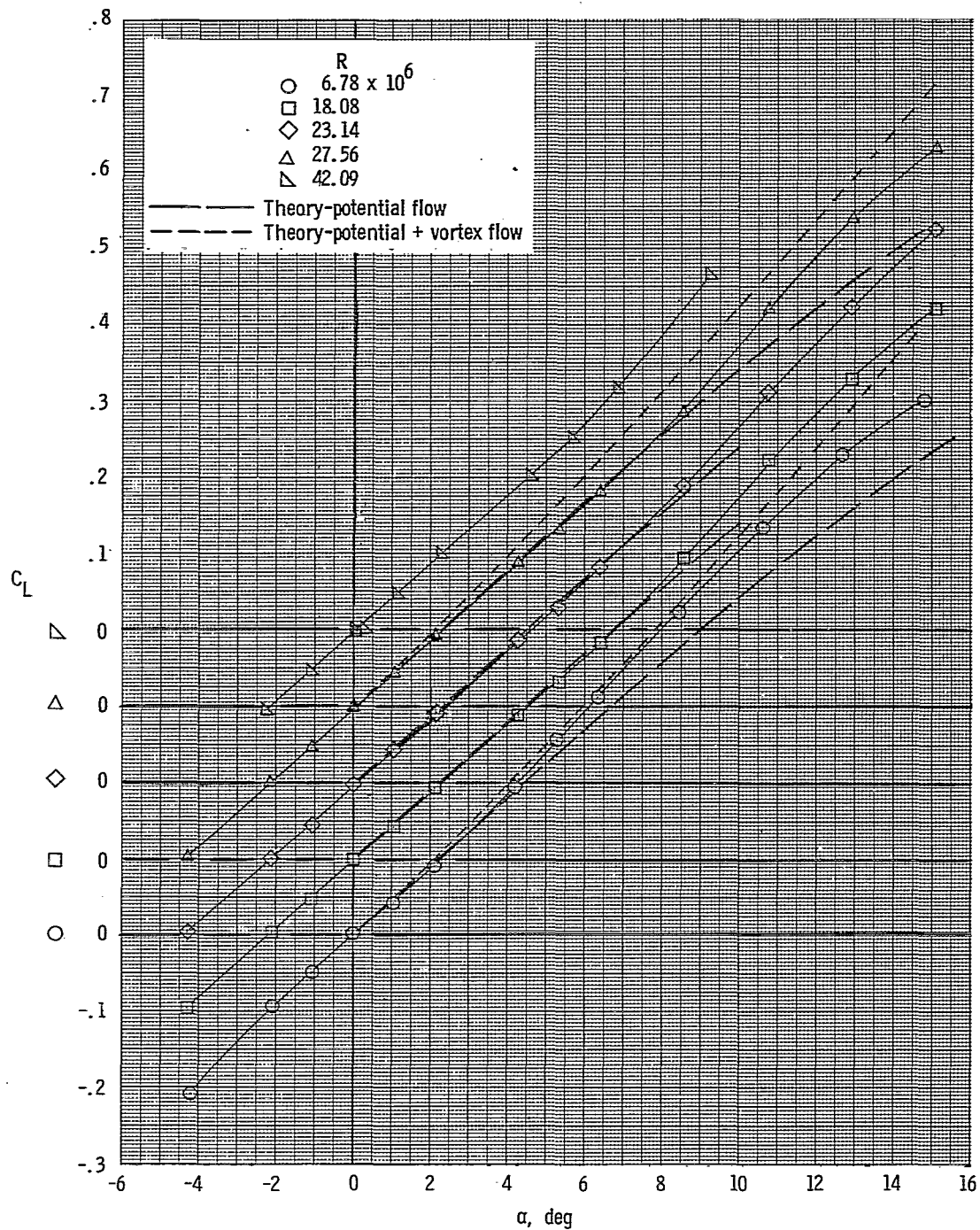


Figure 6.- Effect of Reynolds number on longitudinal aerodynamic characteristics of configuration with leading-edge sweep of  $61.7^\circ$ , trailing-edge sweep of  $40.6^\circ$ , and large leading-edge radius.

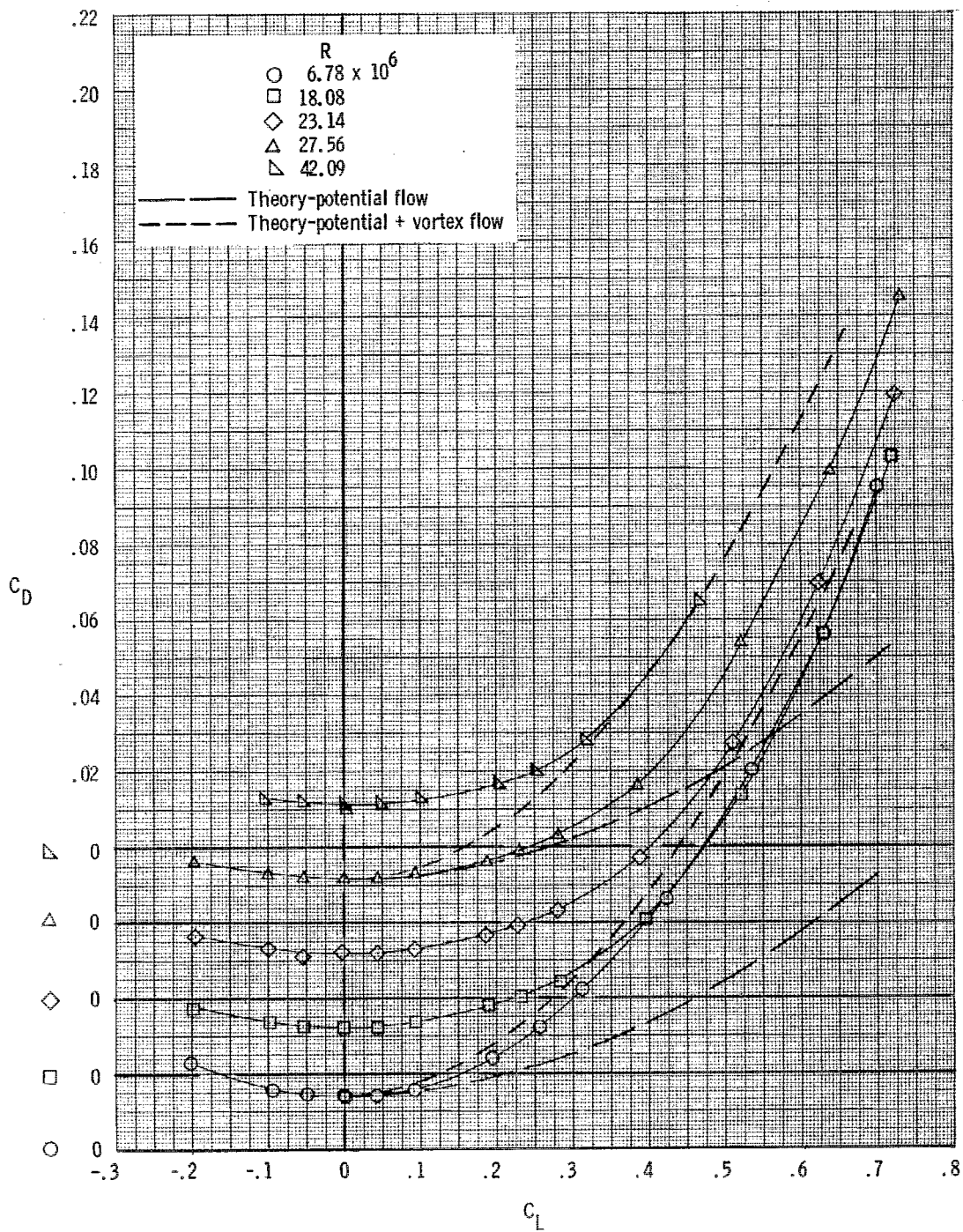


Figure 6.- Continued.

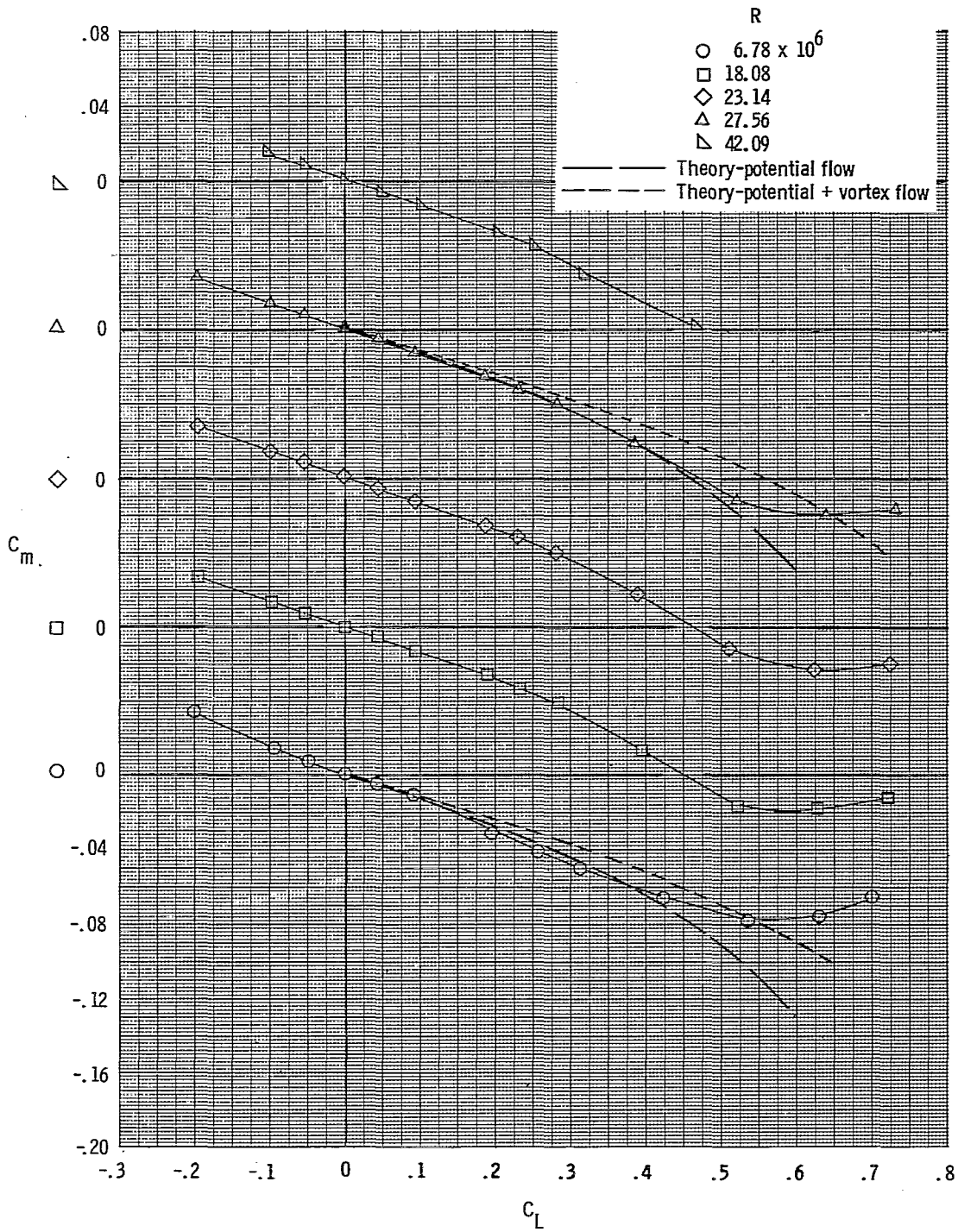


Figure 6.- Concluded.

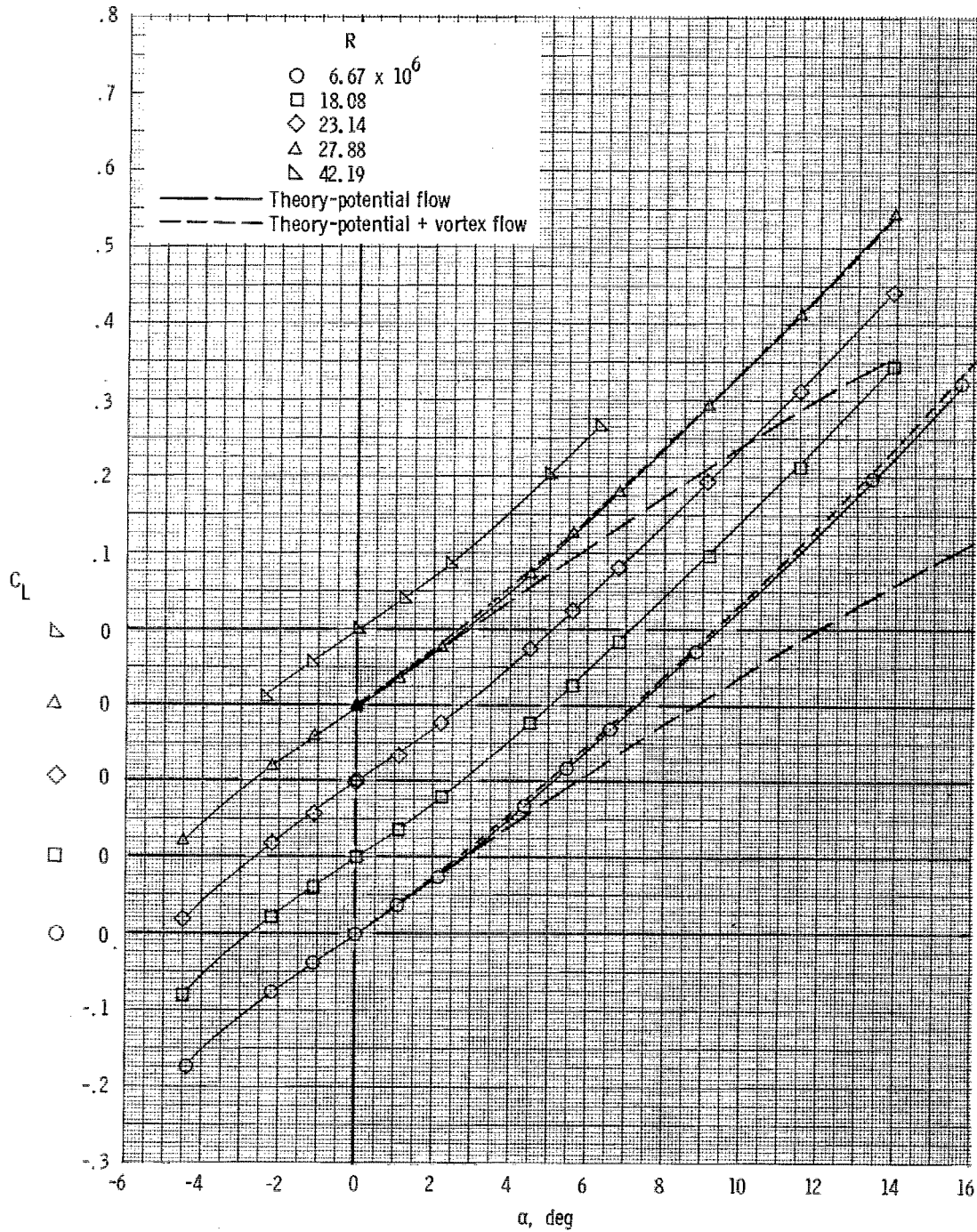


Figure 7.- Effect of Reynolds number on longitudinal aerodynamic characteristics of configuration with leading-edge sweep of  $64.61^\circ$ , trailing-edge sweep of  $0^\circ$ , and sharp leading edge.

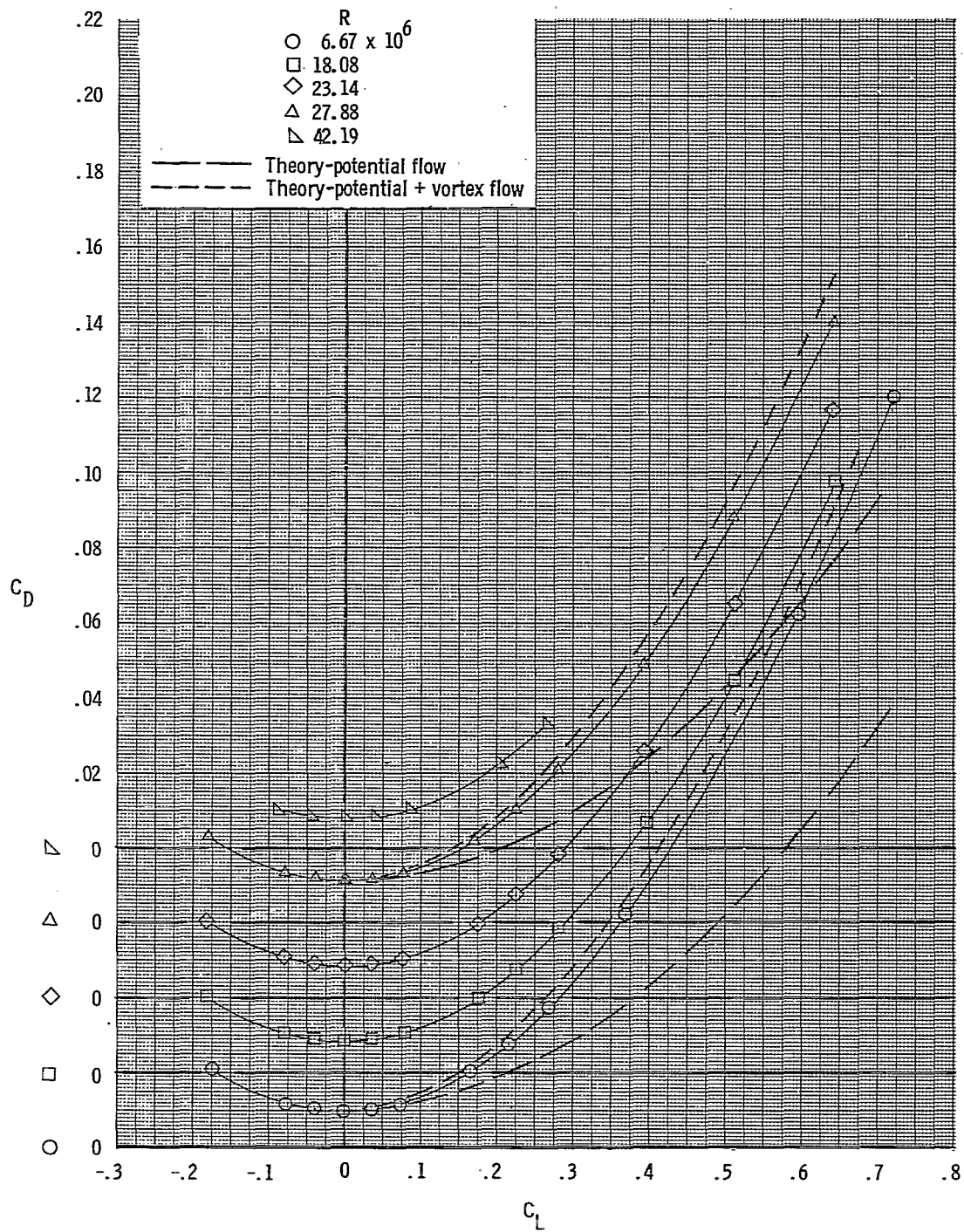


Figure 7.- Continued.

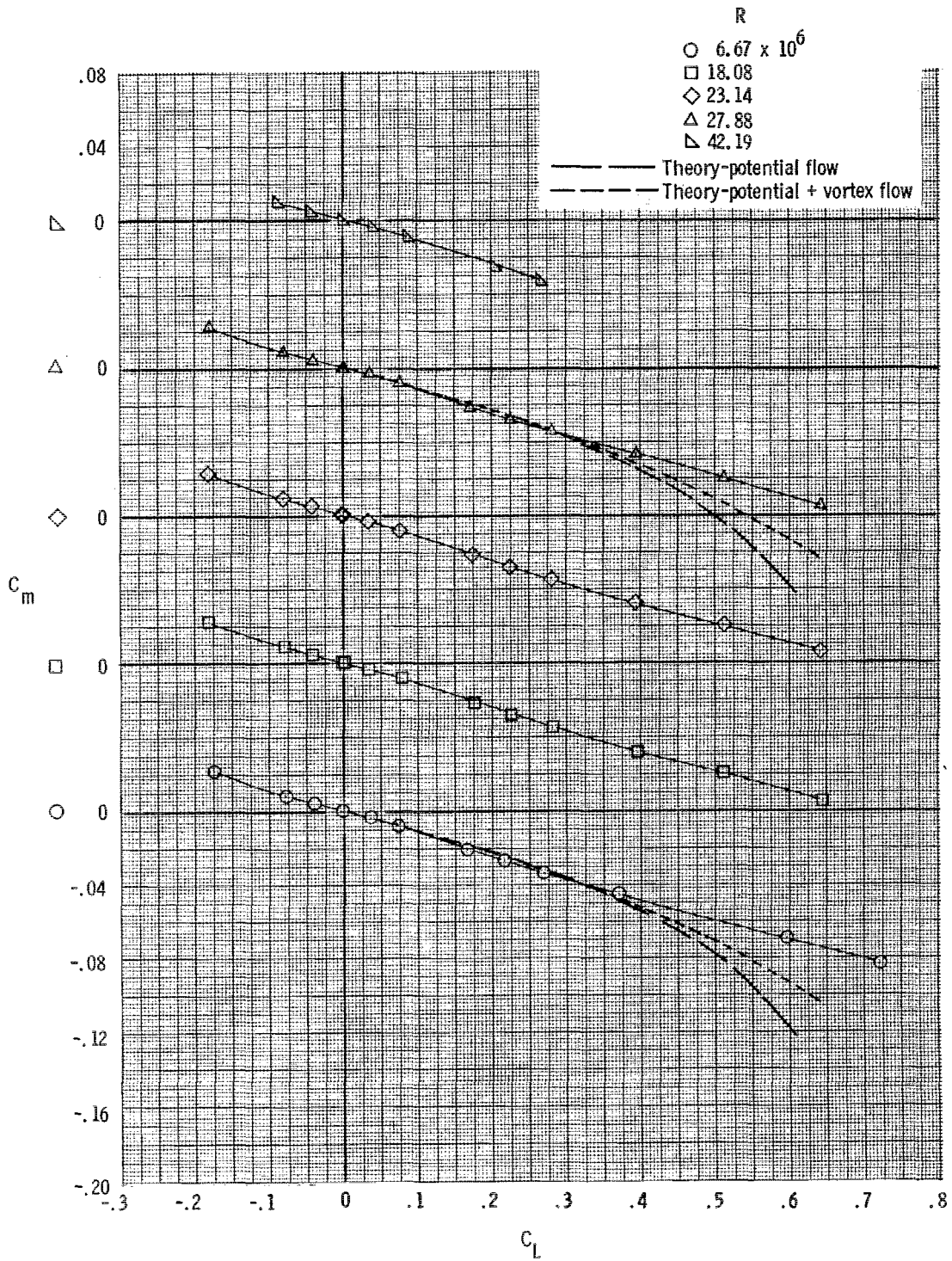


Figure 7.- Concluded.

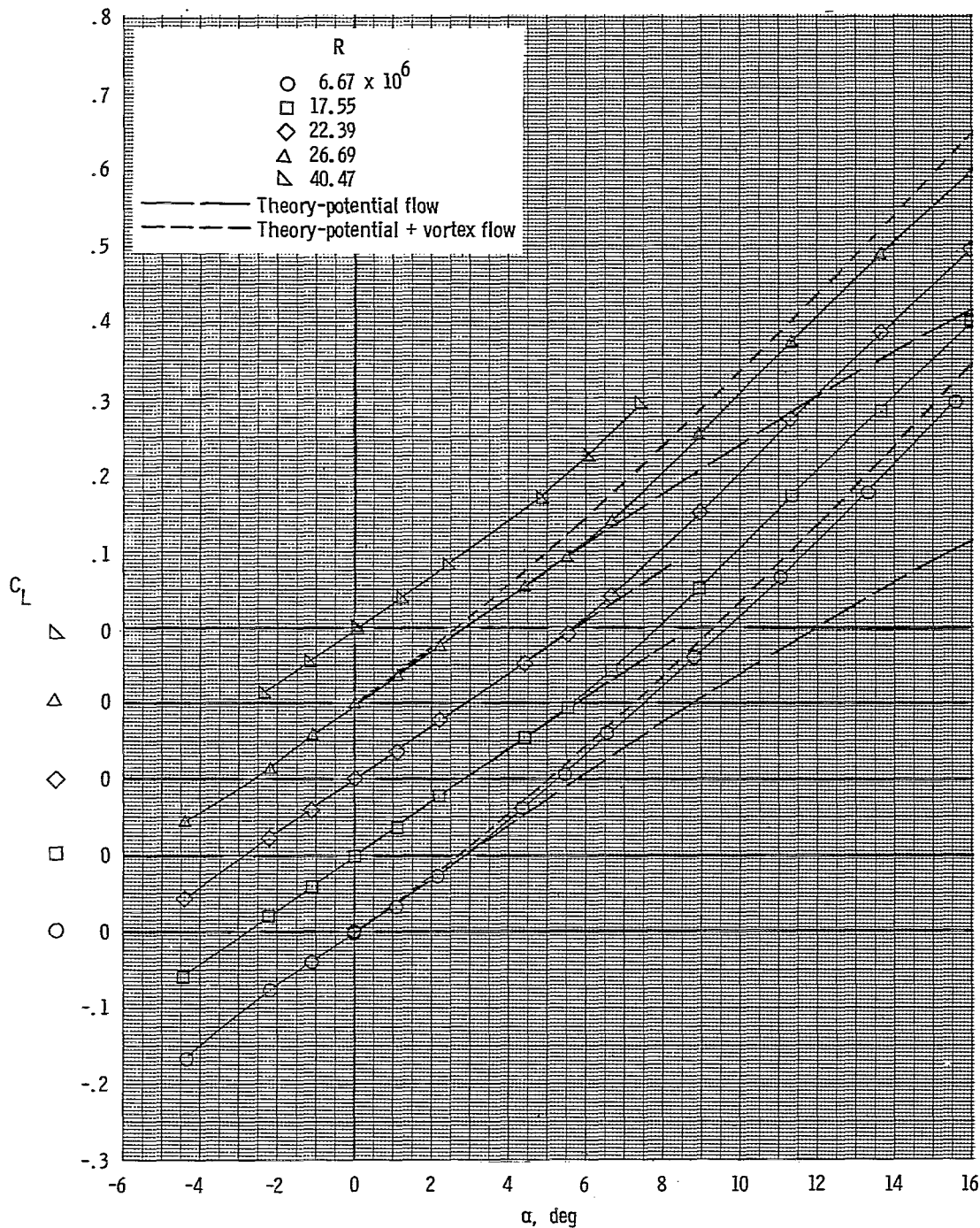


Figure 8.- Effect of Reynolds number on longitudinal aerodynamic characteristics of configuration with leading-edge sweep of  $64.61^\circ$ , trailing-edge sweep of  $0^\circ$ , and large leading-edge radius.

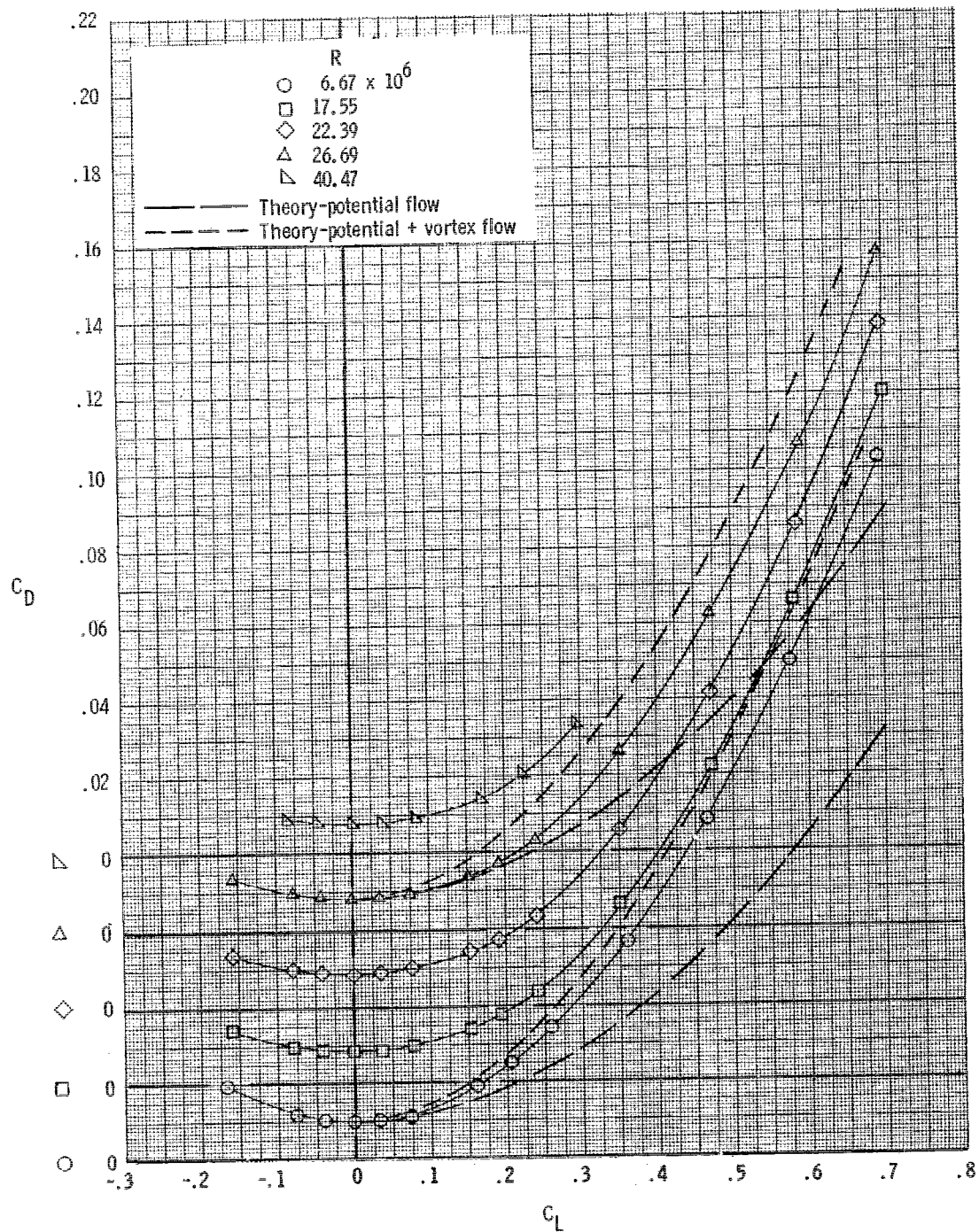


Figure 8.- Continued.

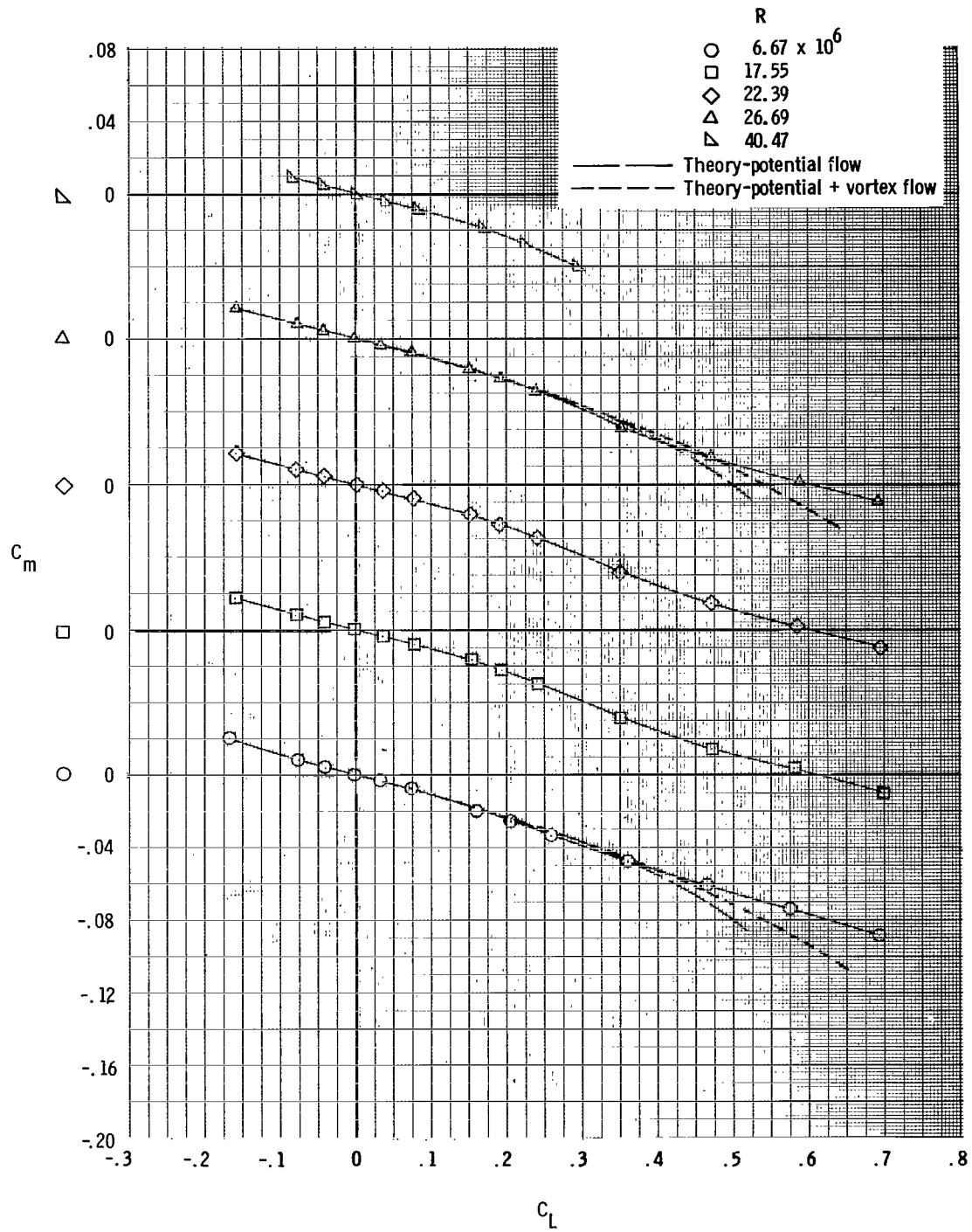


Figure 8.- Concluded.

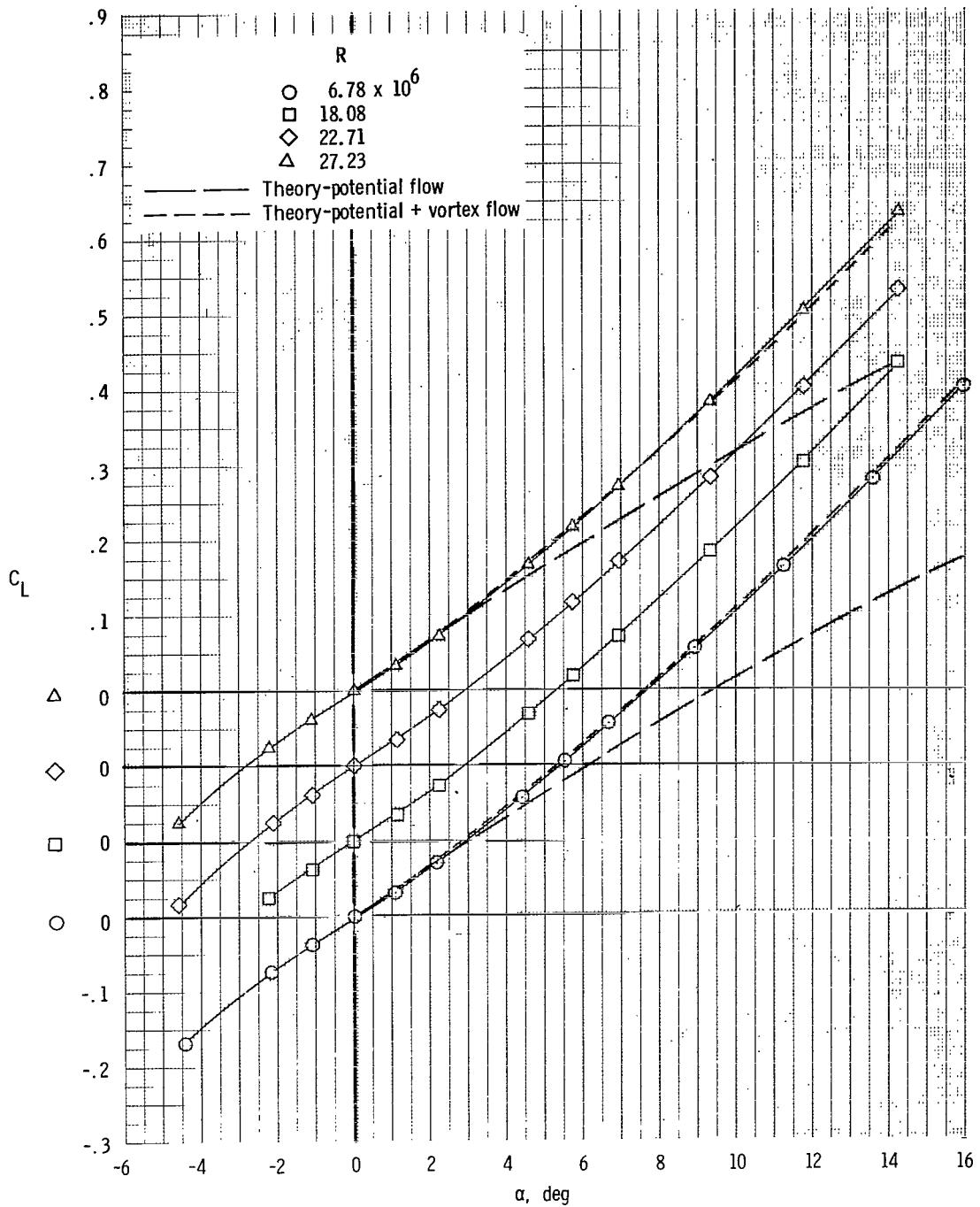


Figure 9.- Effect of Reynolds number on longitudinal aerodynamic characteristics of configuration with leading-edge sweep of  $67.01^\circ$ , trailing-edge sweep of  $0^\circ$ , and sharp leading edge.

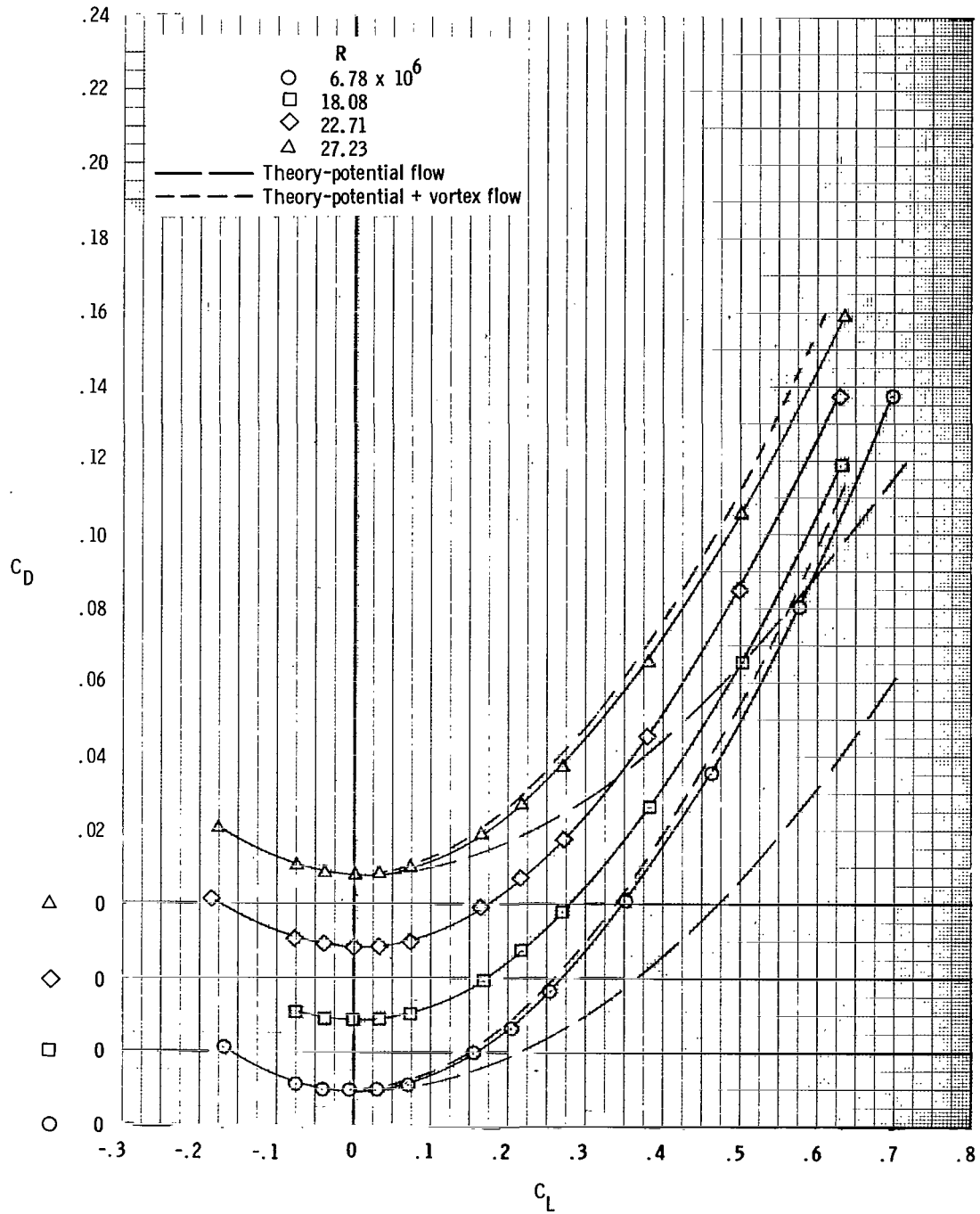


Figure 9.- Continued.

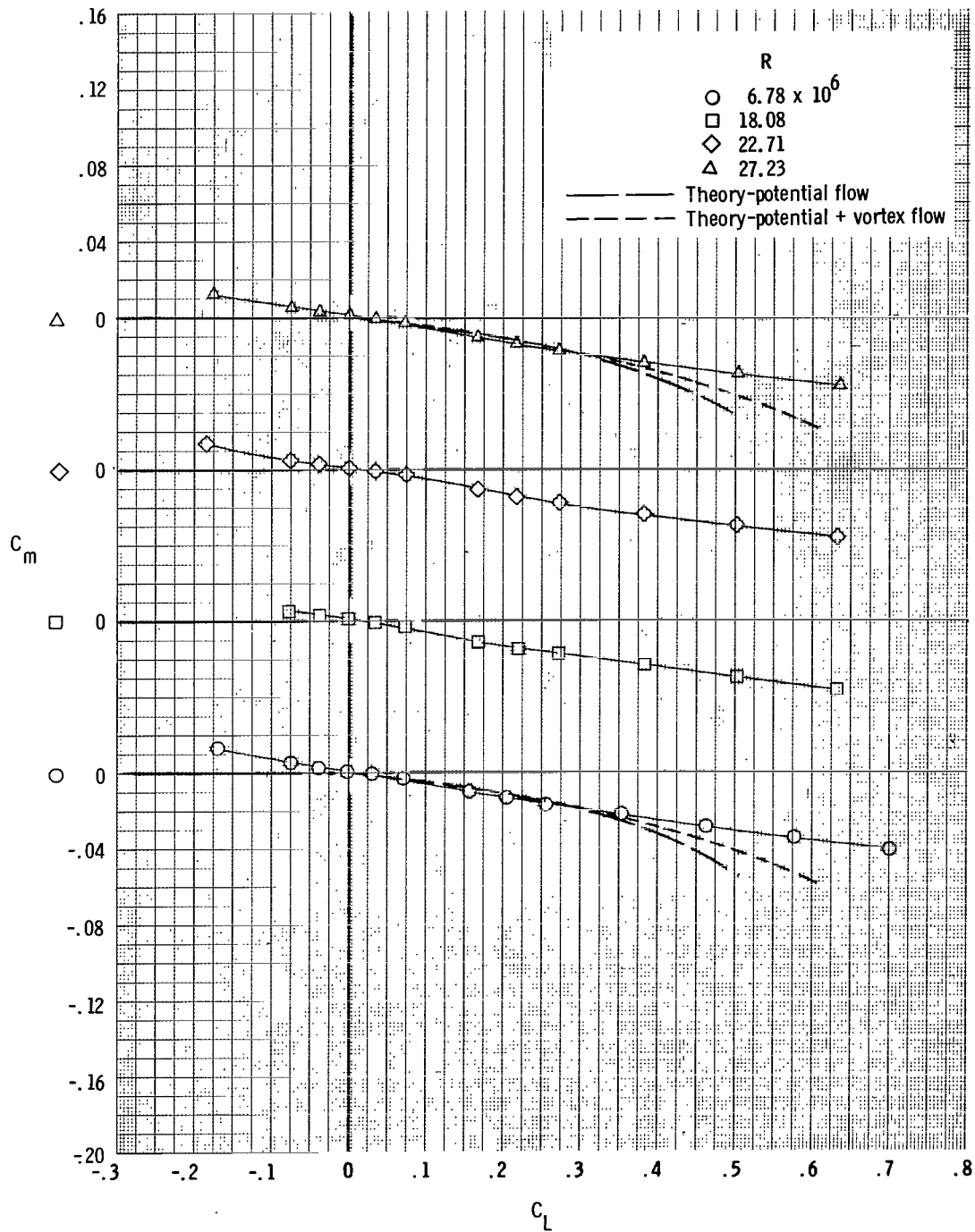


Figure 9.- Concluded.

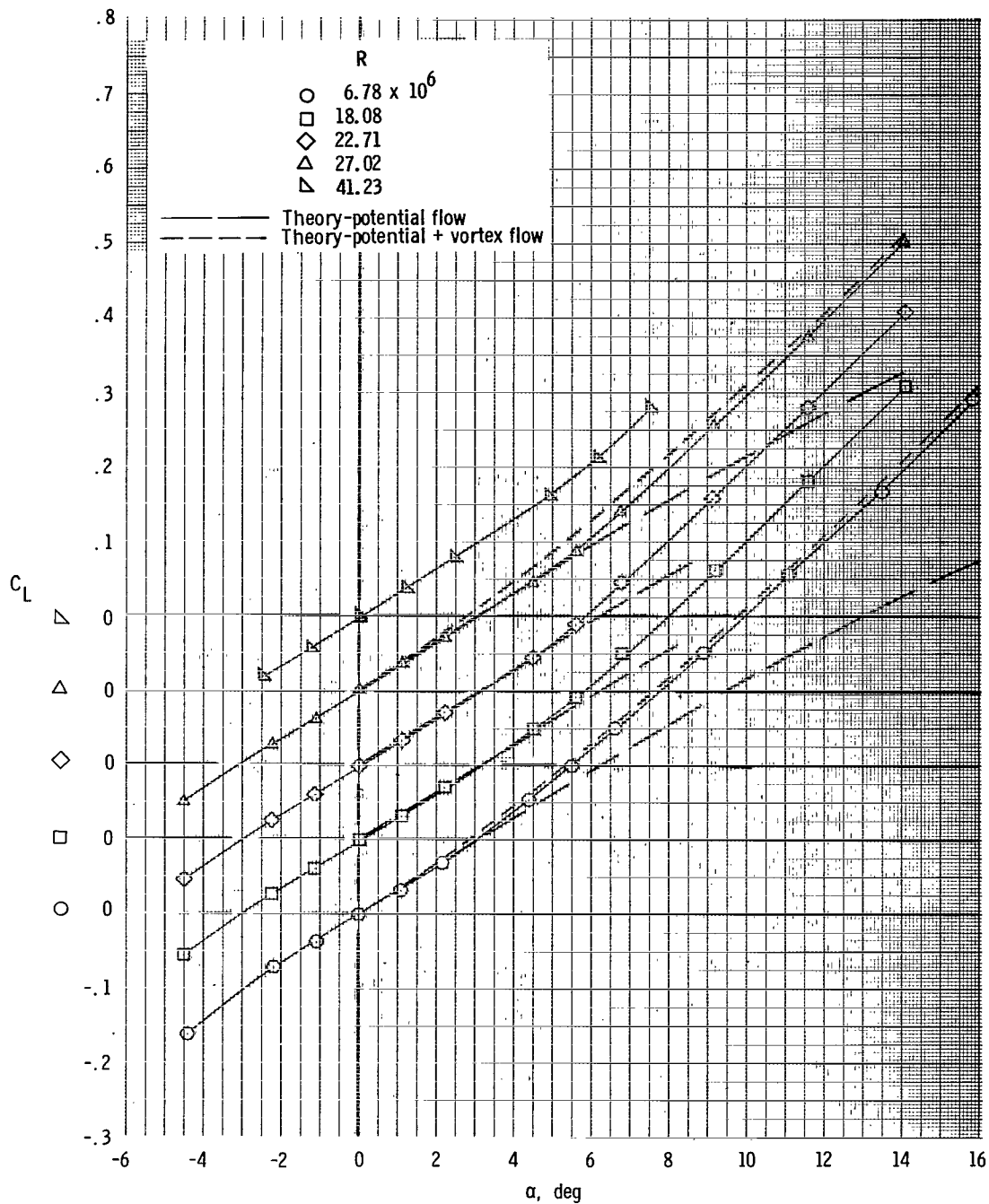


Figure 10.- Effect of Reynolds number on the longitudinal aerodynamic characteristics of configuration with leading-edge sweep of  $67.01^\circ$ , trailing-edge sweep of  $0^\circ$ , and small leading-edge radius.

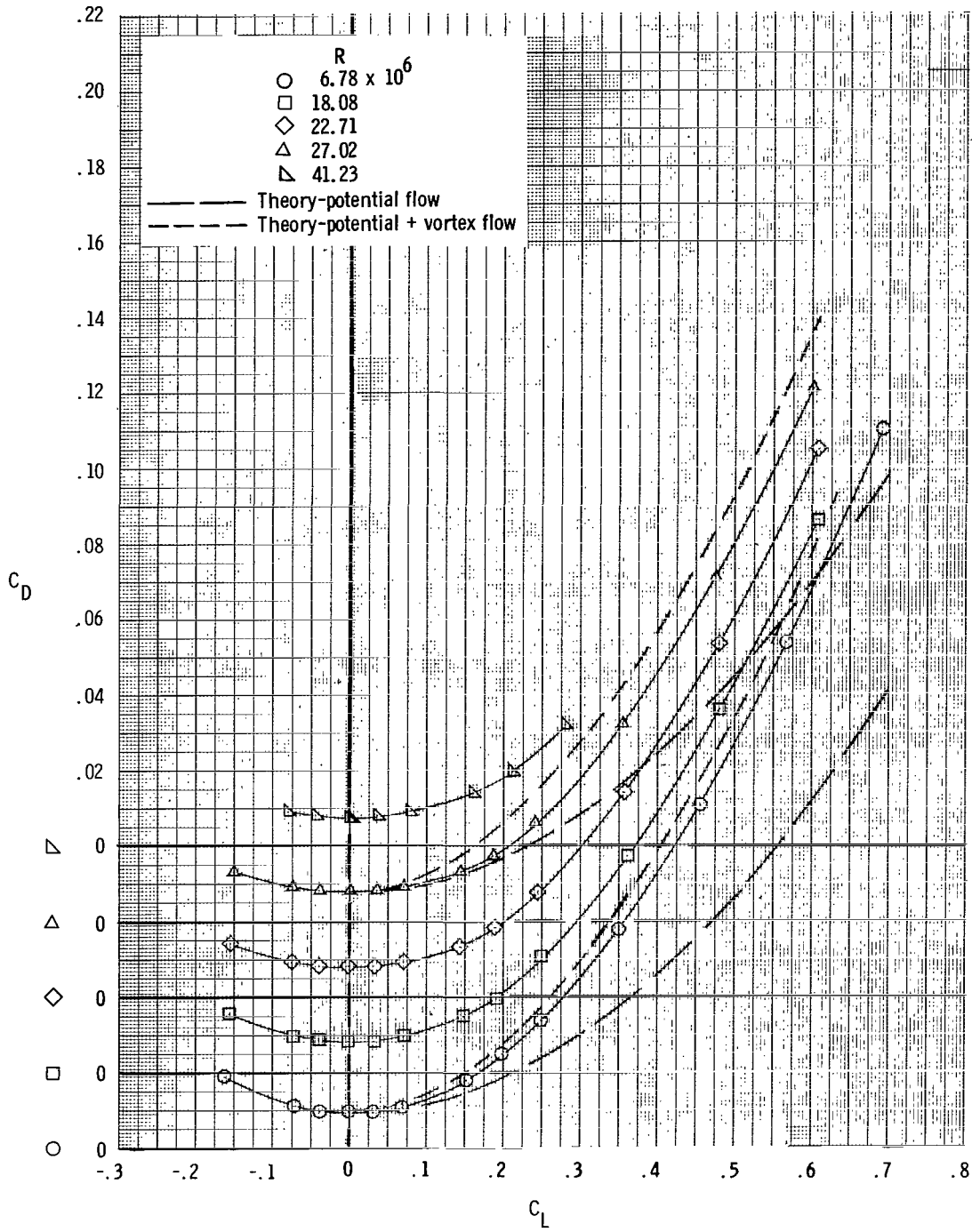


Figure 10.- Continued.

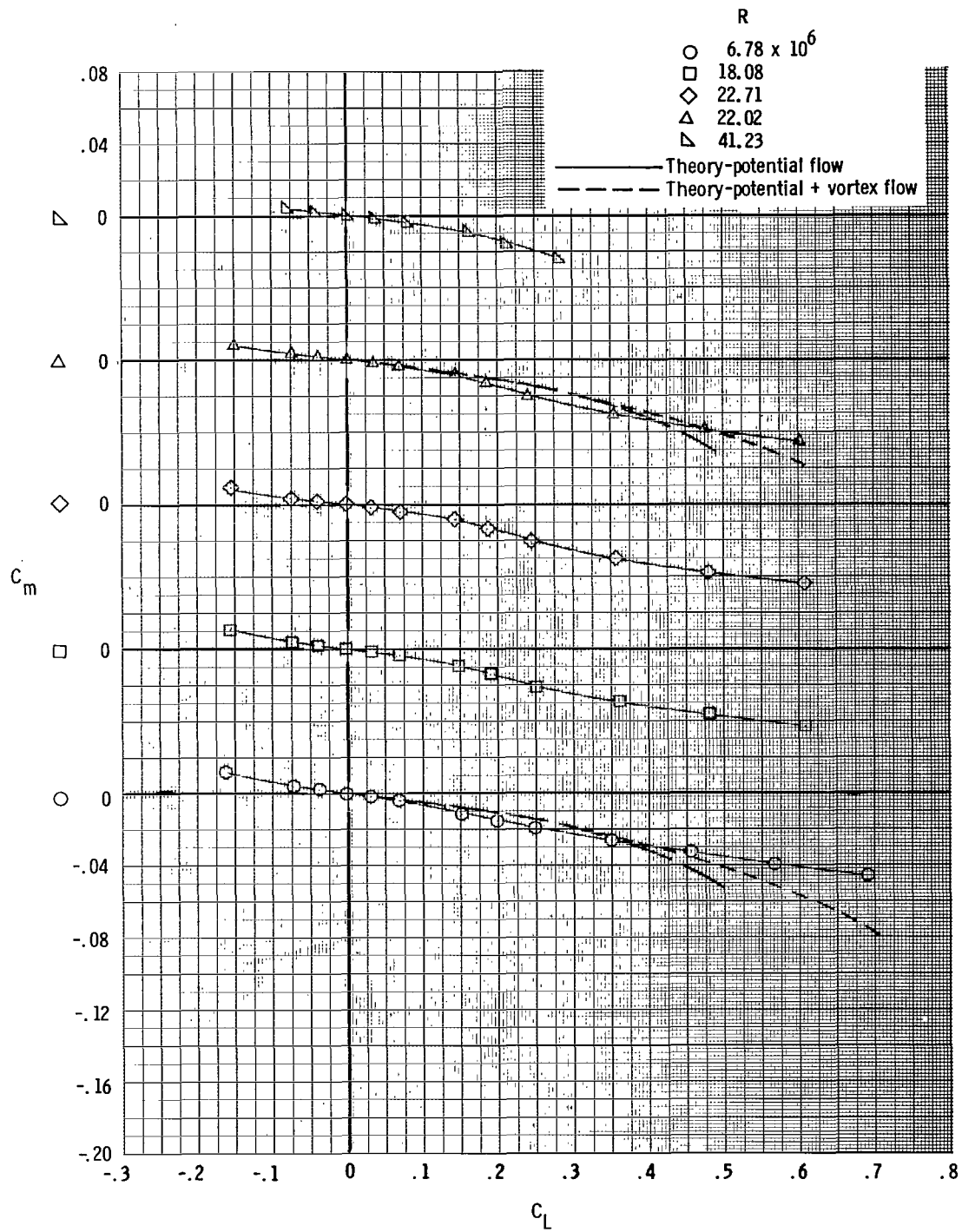


Figure 10.- Concluded.

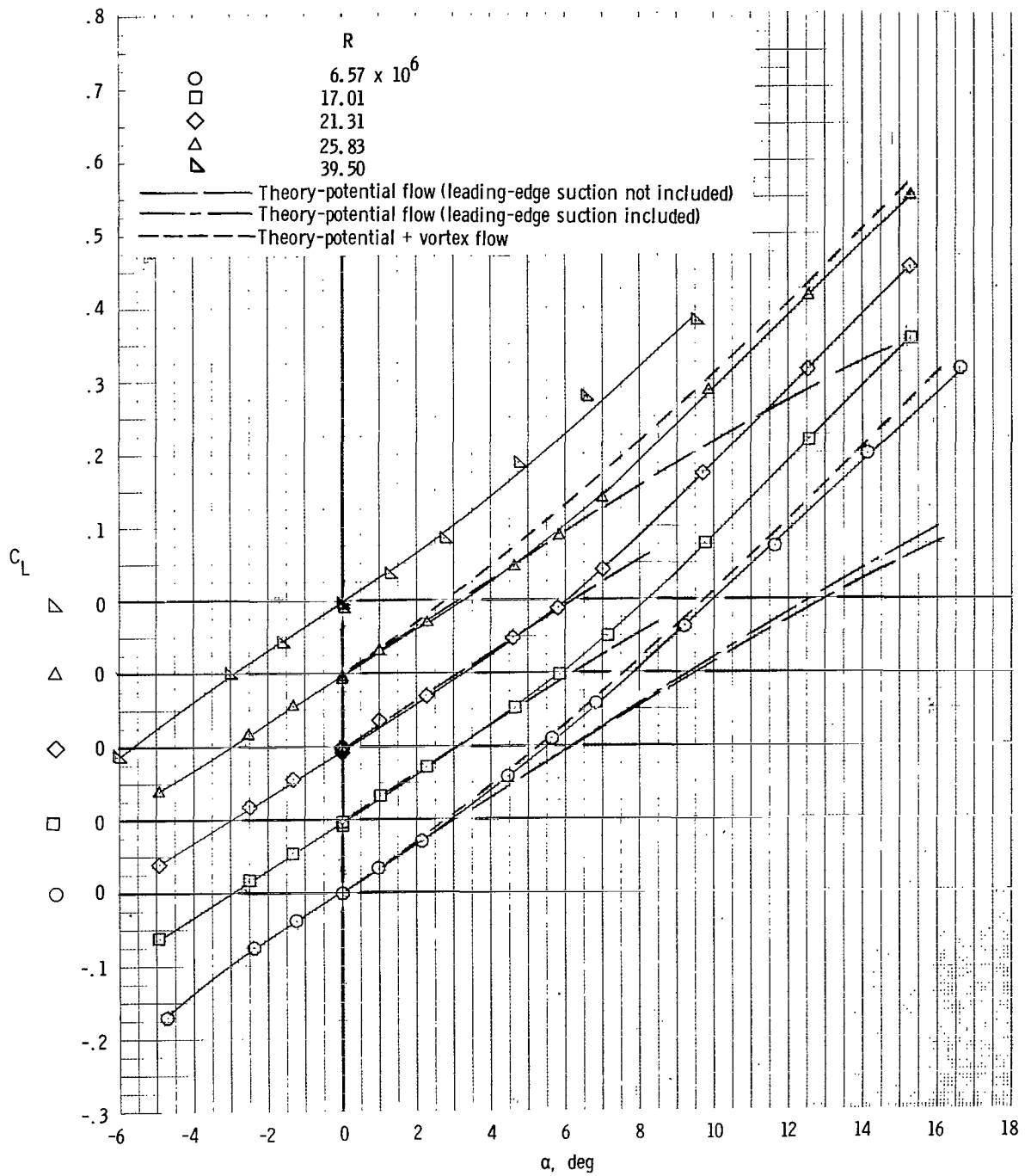


Figure 11.- Effect of Reynolds number on the longitudinal aerodynamic characteristics of configuration with leading-edge sweep of  $67.01^\circ$ , trailing-edge sweep of  $0^\circ$ , and large leading-edge radius.

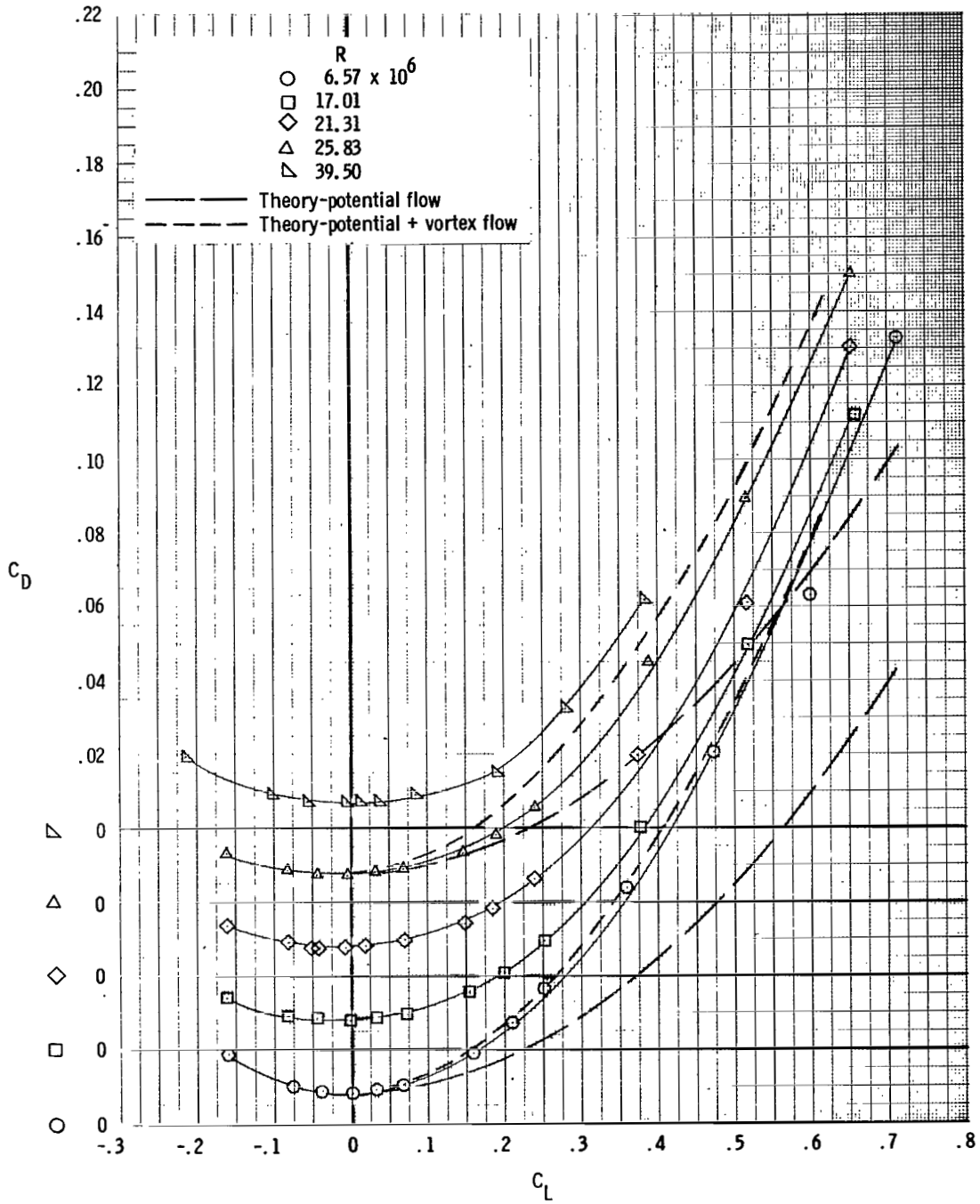


Figure 11.- Continued.

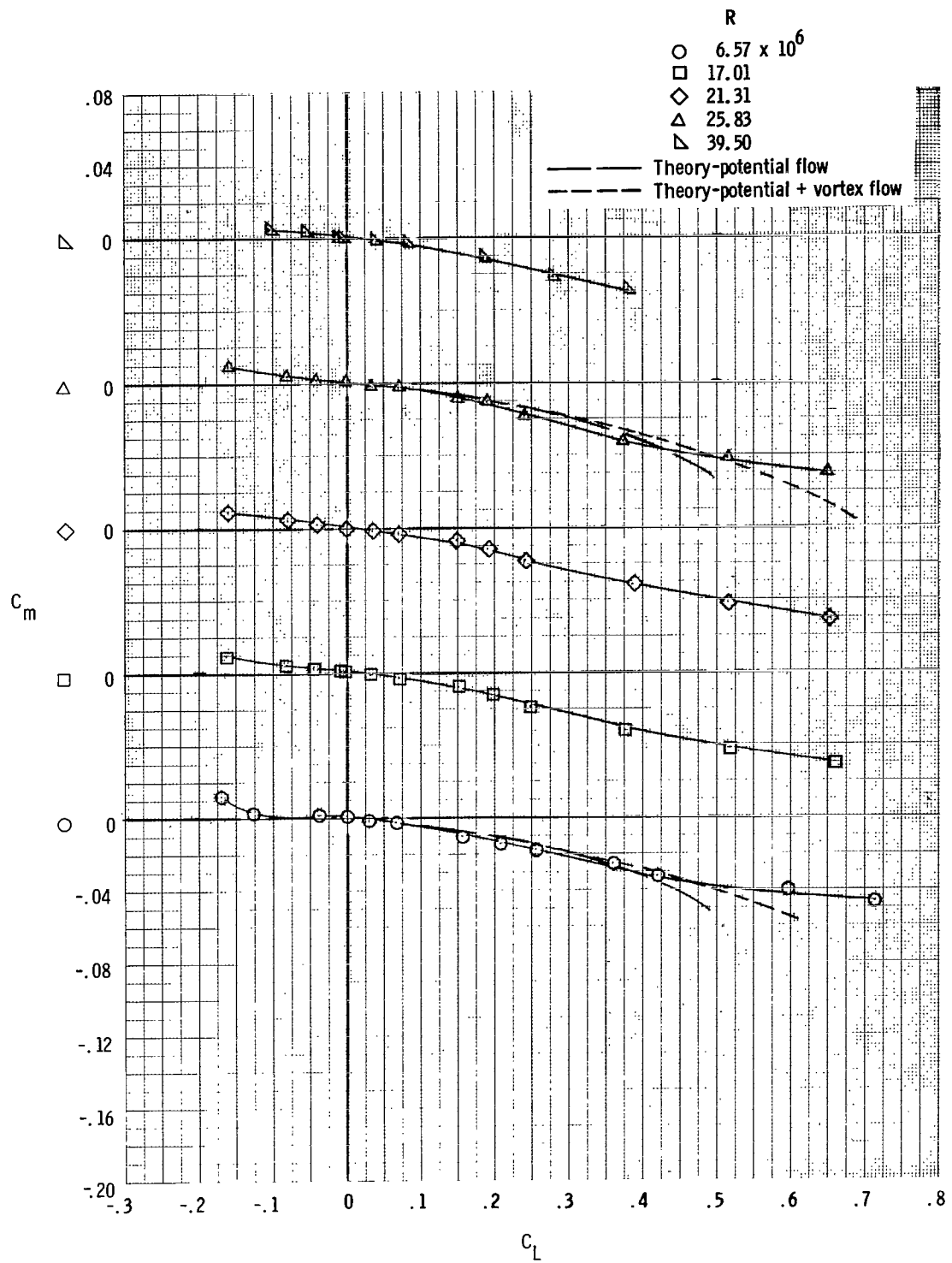


Figure 11.- Concluded.

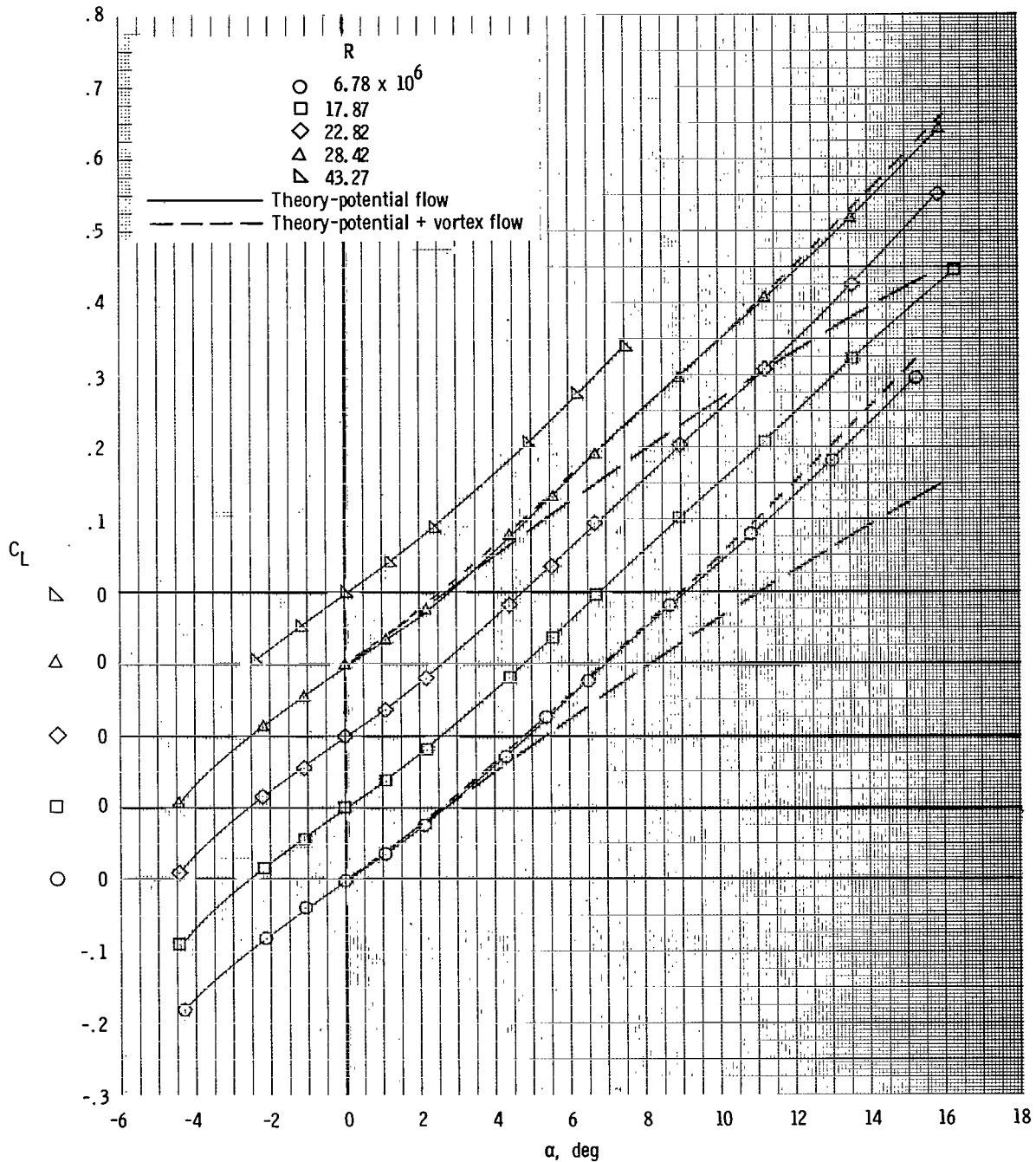


Figure 12.- Effect of Reynolds number on the longitudinal aerodynamic characteristics of the configuration with leading-edge sweep of  $67.01^\circ$ , trailing-edge sweep of  $40.6^\circ$ , and sharp leading edge.

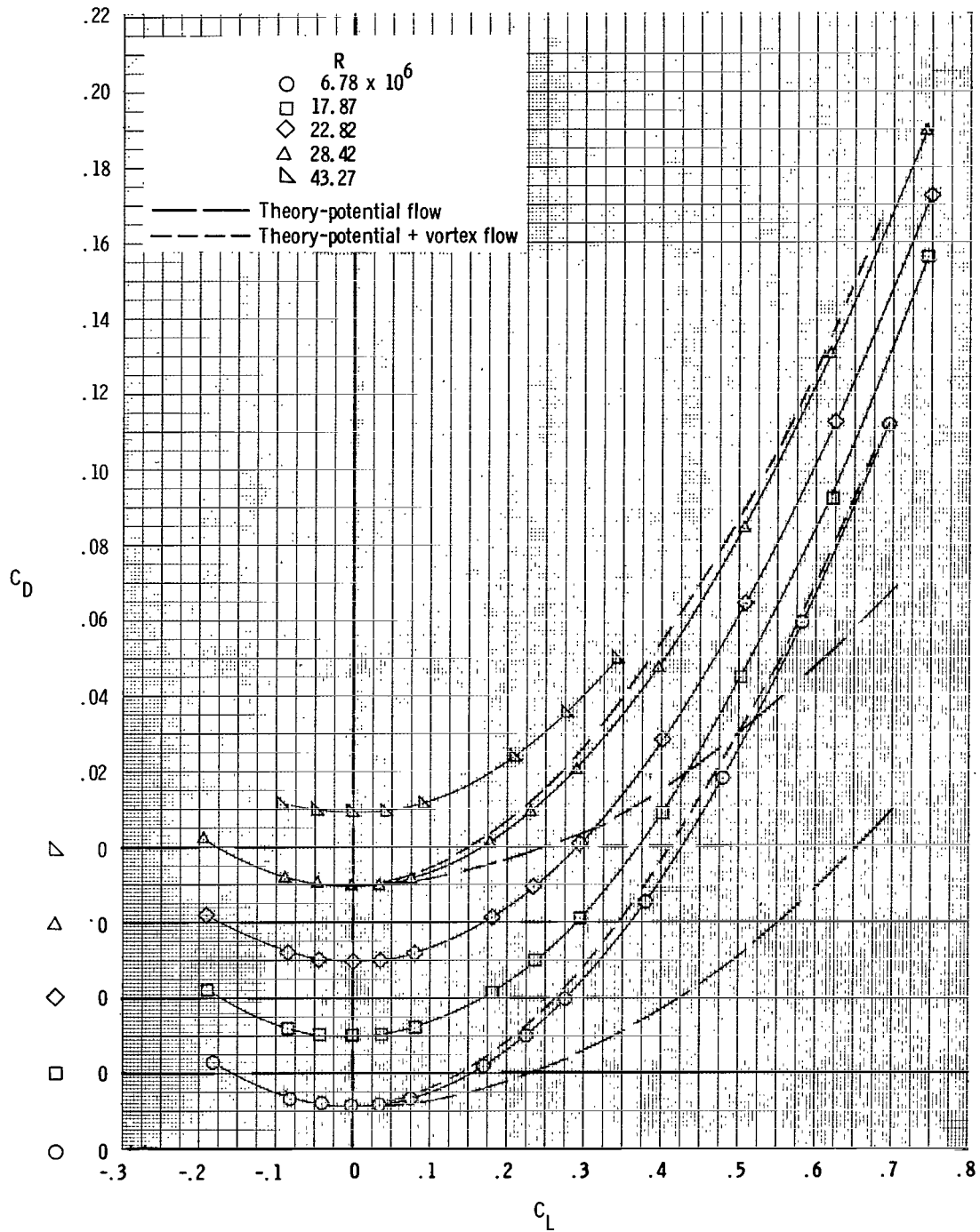


Figure 12.- Continued.

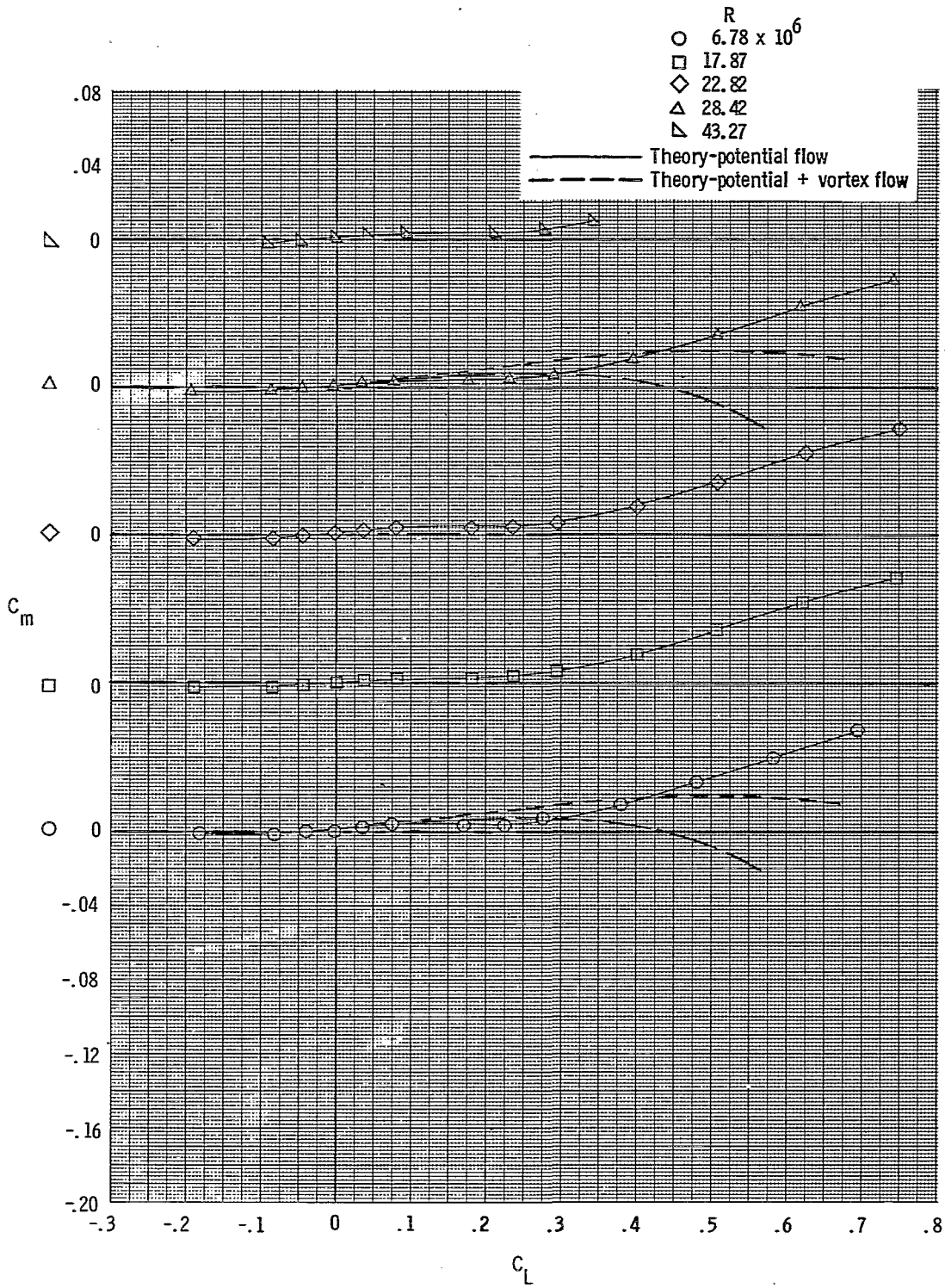


Figure 12.- Concluded.

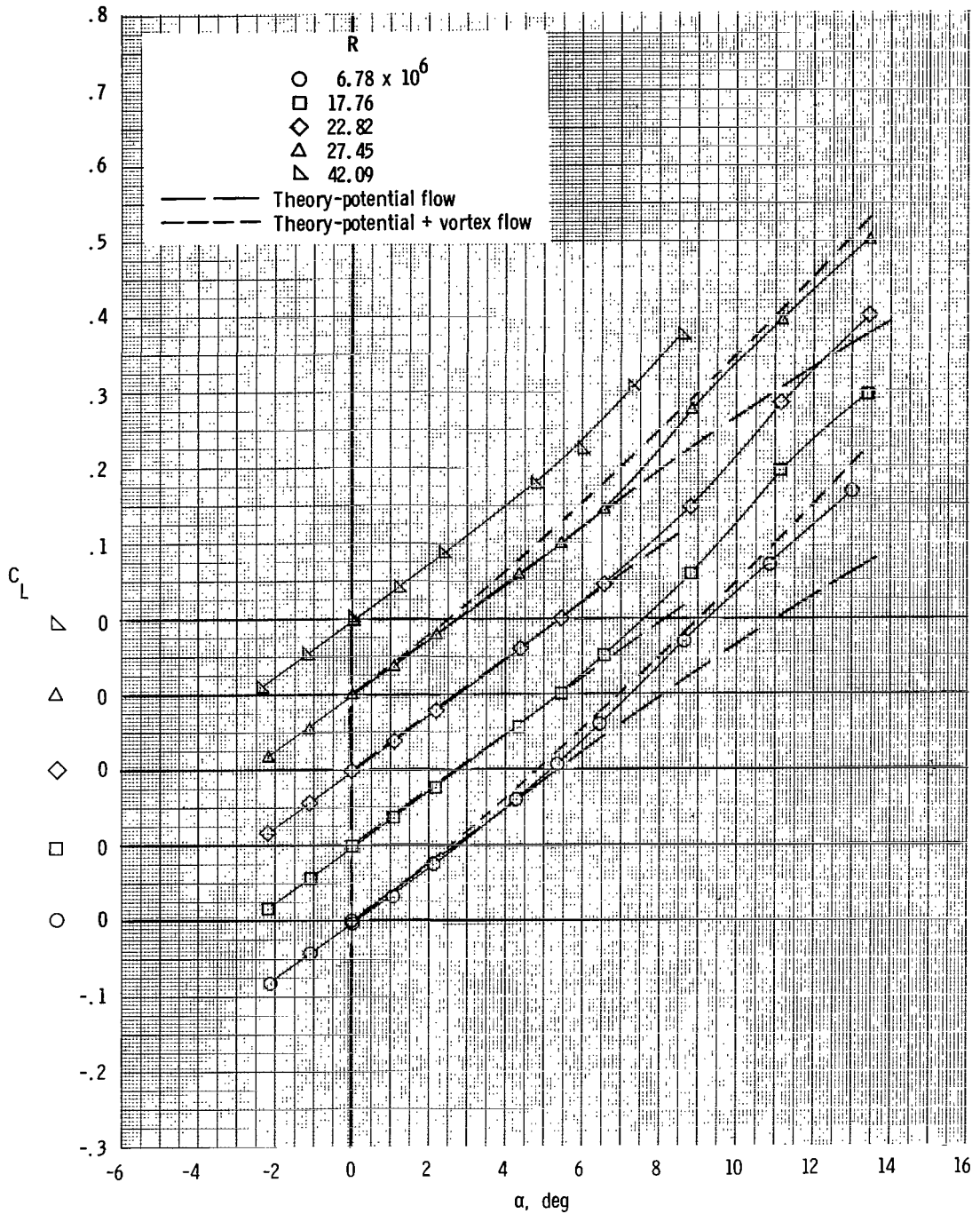


Figure 13.- Effect of Reynolds number on the longitudinal aerodynamic characteristics of configuration with leading-edge sweep of  $67.01^\circ$ , trailing-edge sweep of  $40.6^\circ$ , and large leading-edge radius.

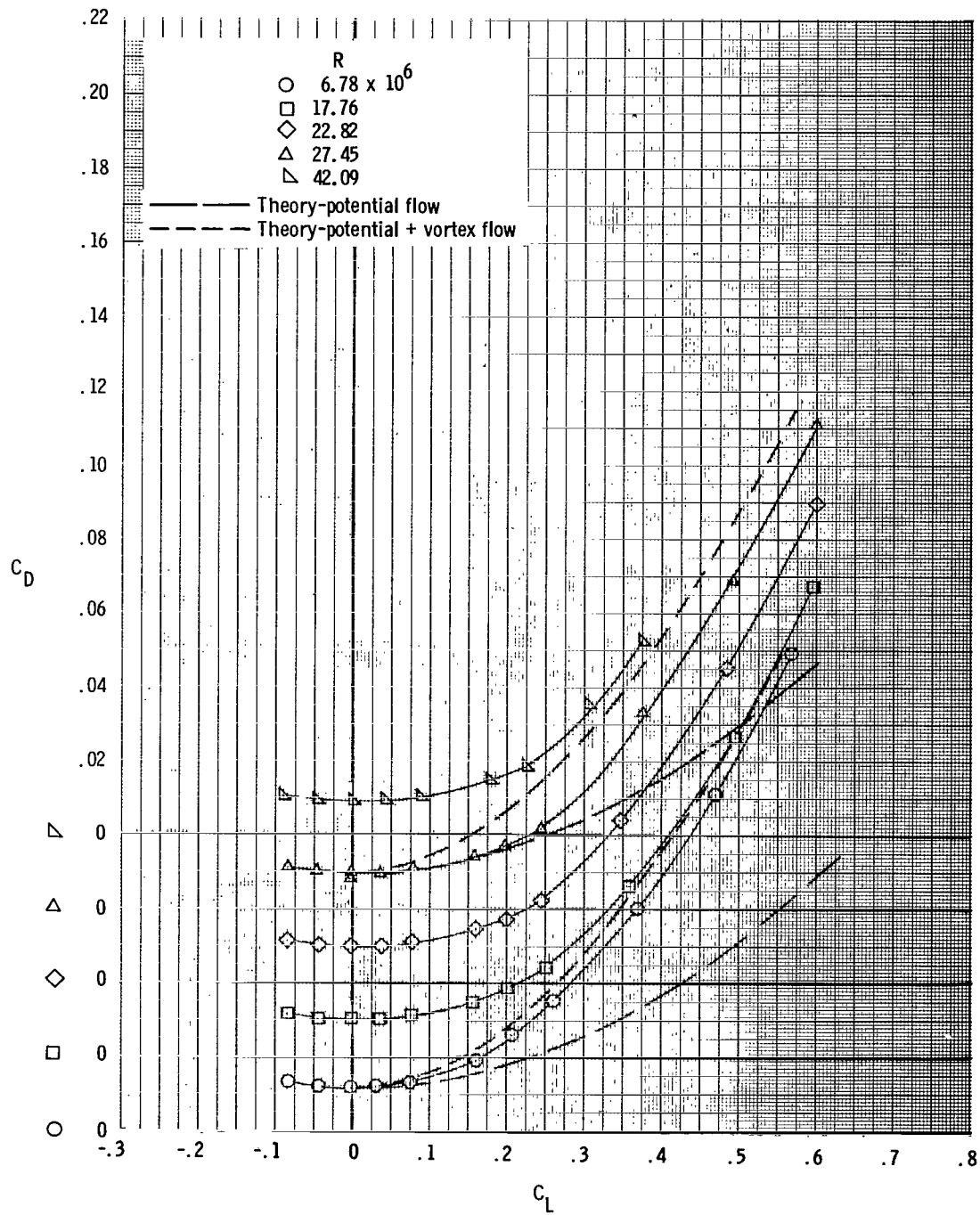


Figure 13.- Continued.

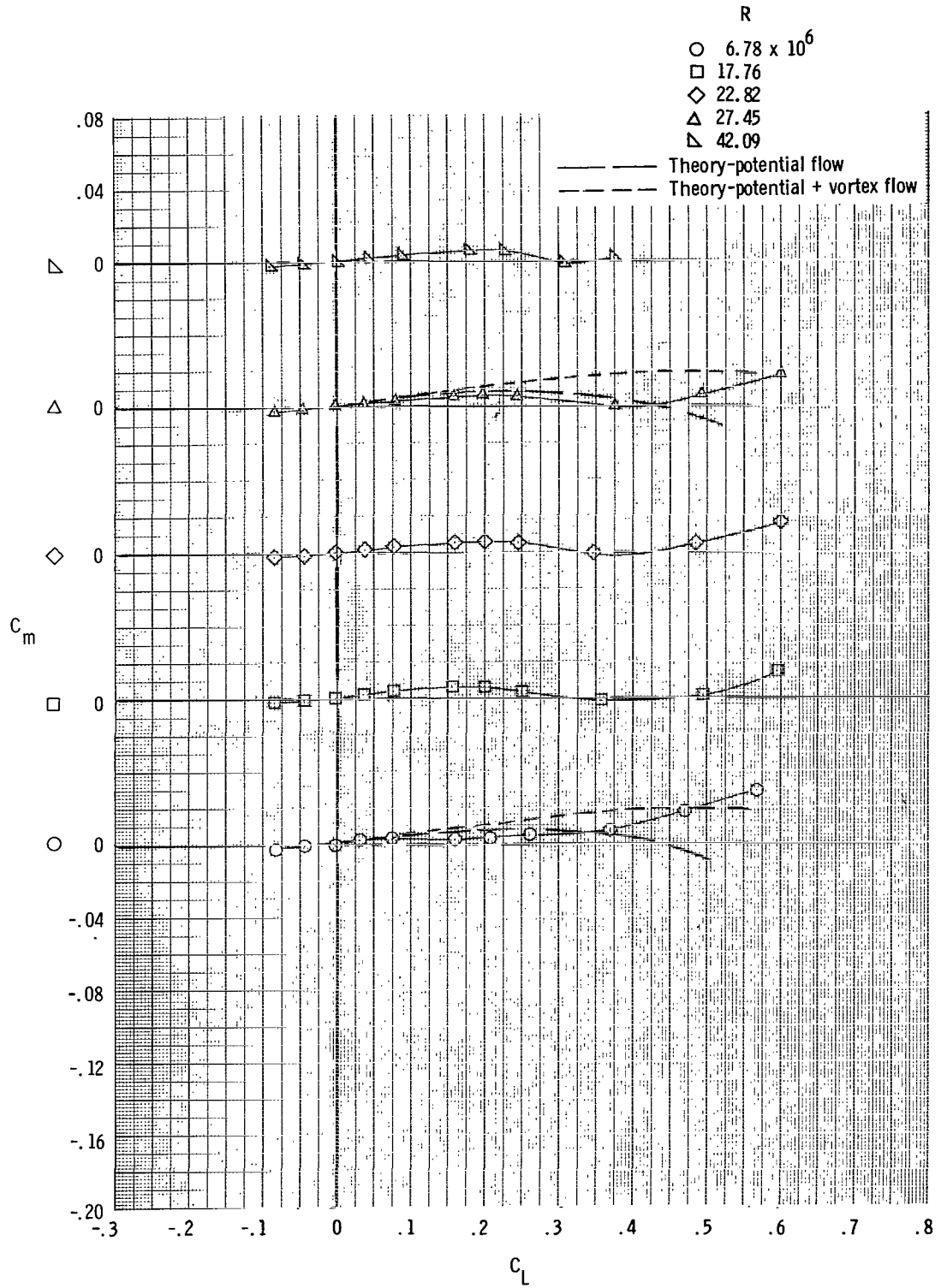


Figure 13.- Concluded.

Experiment  
 ○  
 □

Vortex-lift contributions to normal force from:  
 - - - Leading edge  
 — Leading edge plus augmented

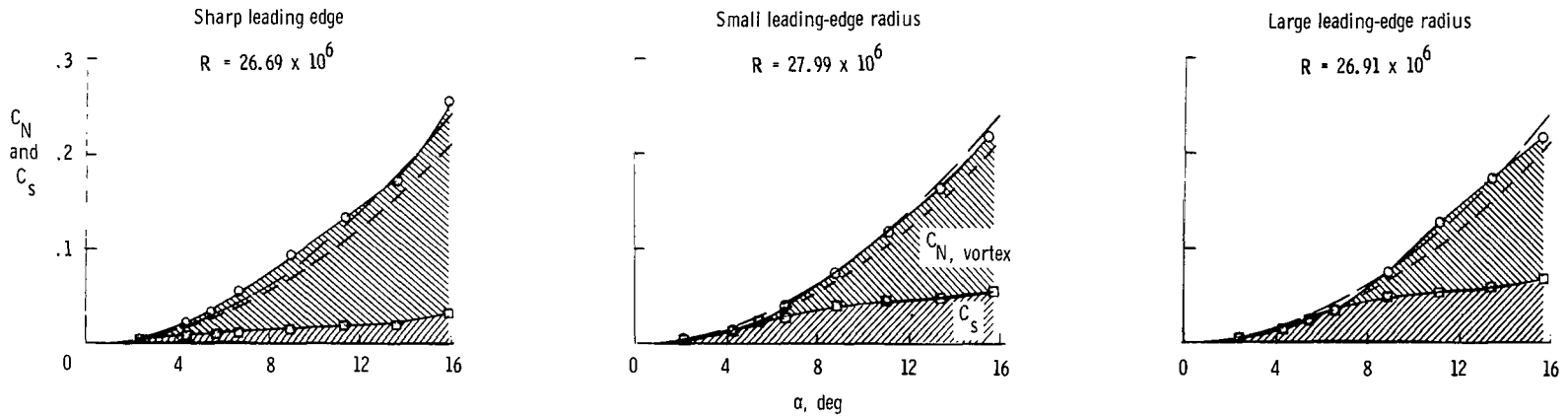


Figure 14.- Effect of leading-edge profile on leading-edge vortex flow characteristics for configuration with leading-edge sweep of  $61.7^\circ$  and trailing-edge sweep of  $0^\circ$ .

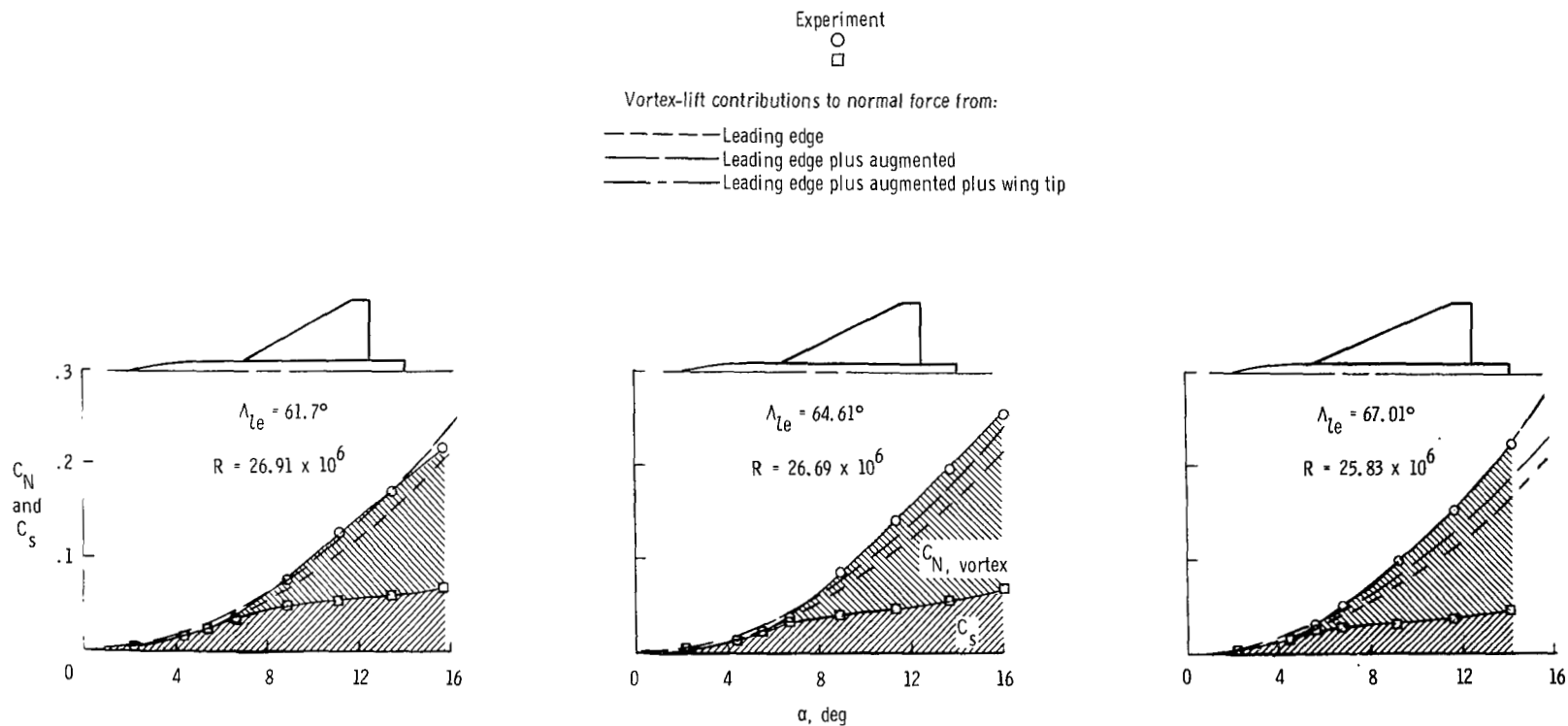


Figure 15.- Effect of leading-edge sweep on leading-edge vortex flow characteristics for configuration with trailing-edge sweep of  $0^\circ$ .

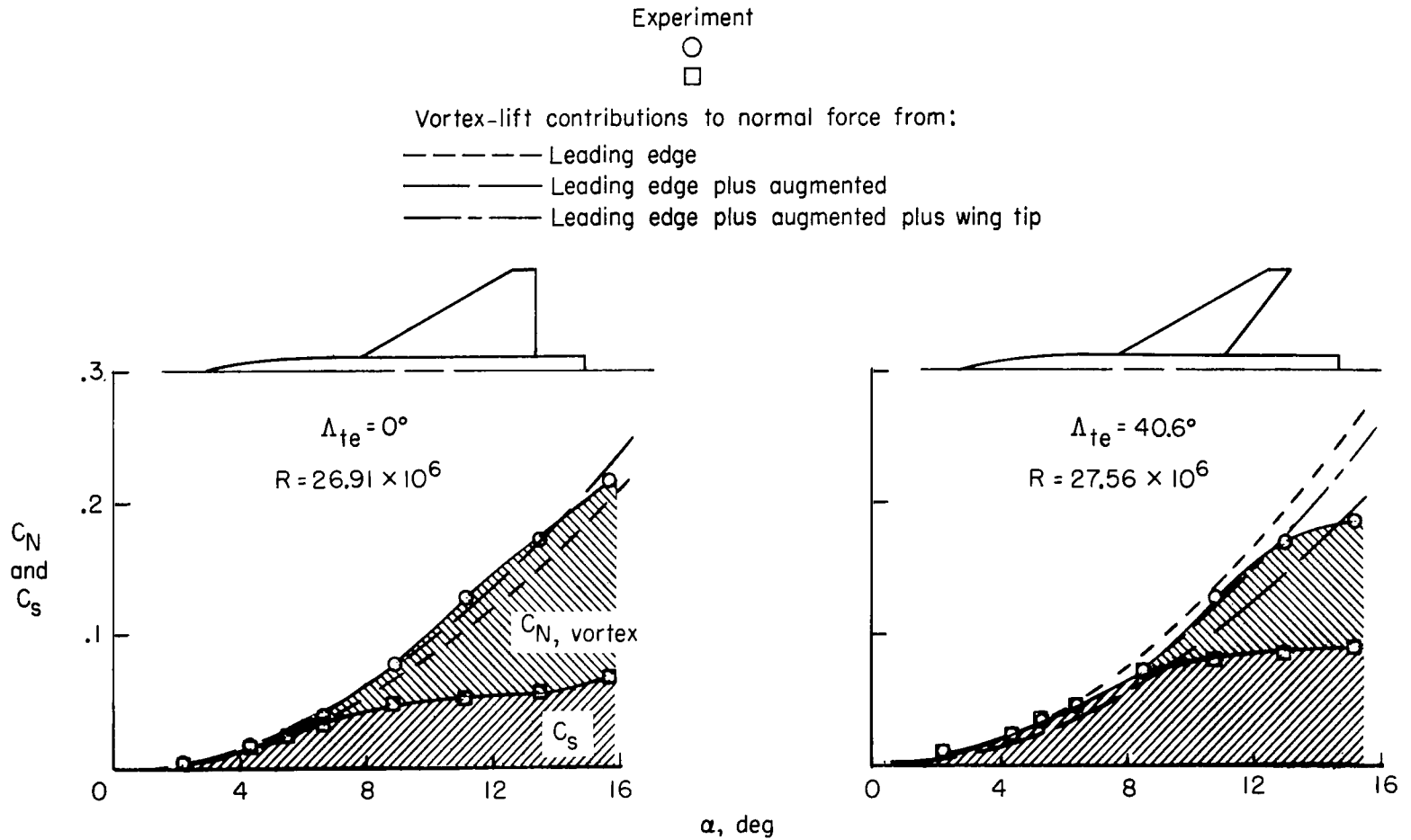


Figure 16.- Effect of trailing-edge sweep on leading-edge vortex flow characteristics for configuration with leading-edge sweep of  $61.7^\circ$  and large leading-edge radius.

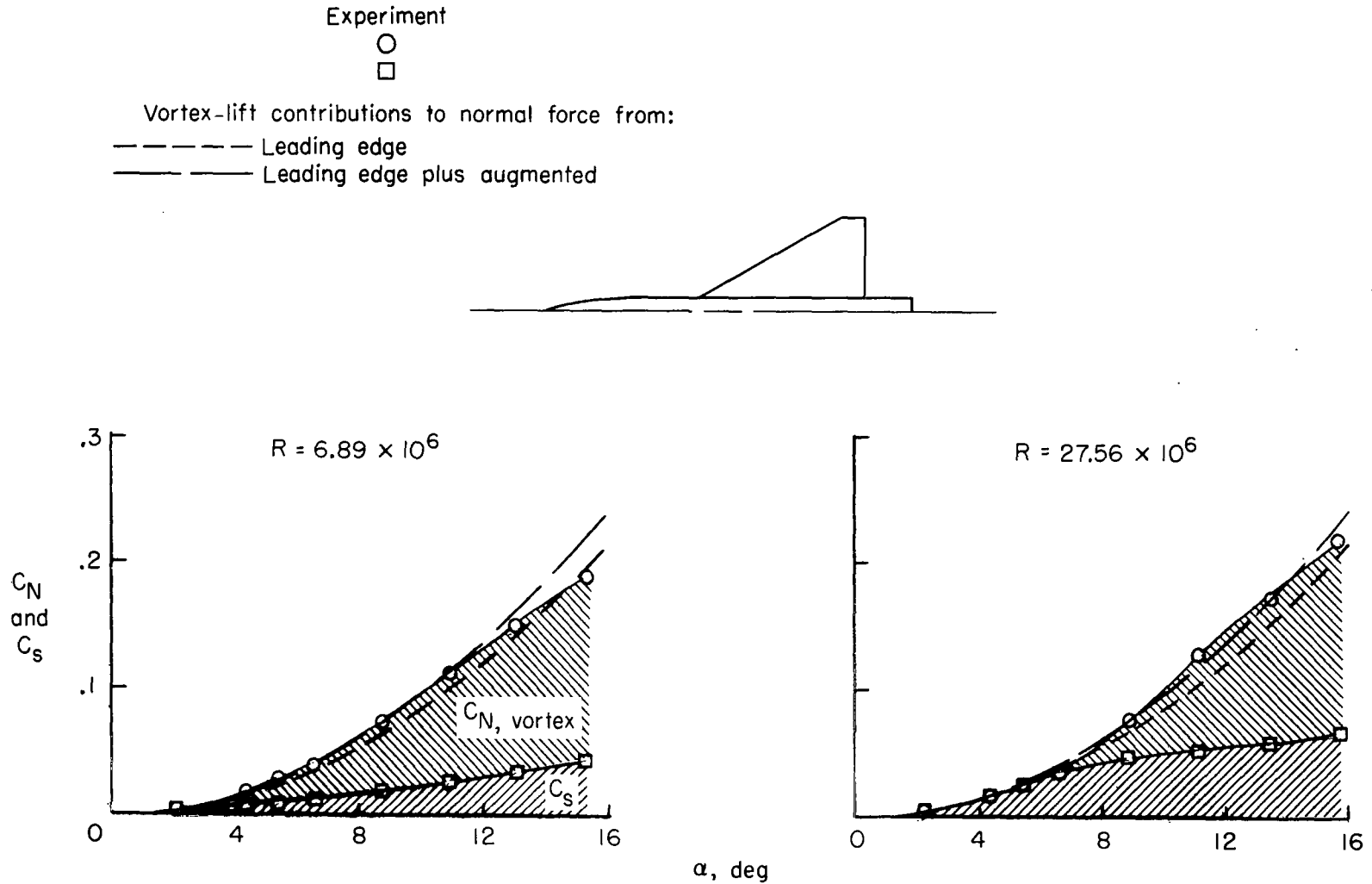


Figure 17.- Effect of Reynolds number on leading-edge vortex flow characteristics for configuration with leading-edge sweep of  $61.7^\circ$ , trailing-edge sweep of  $0^\circ$ , and large leading-edge radius.

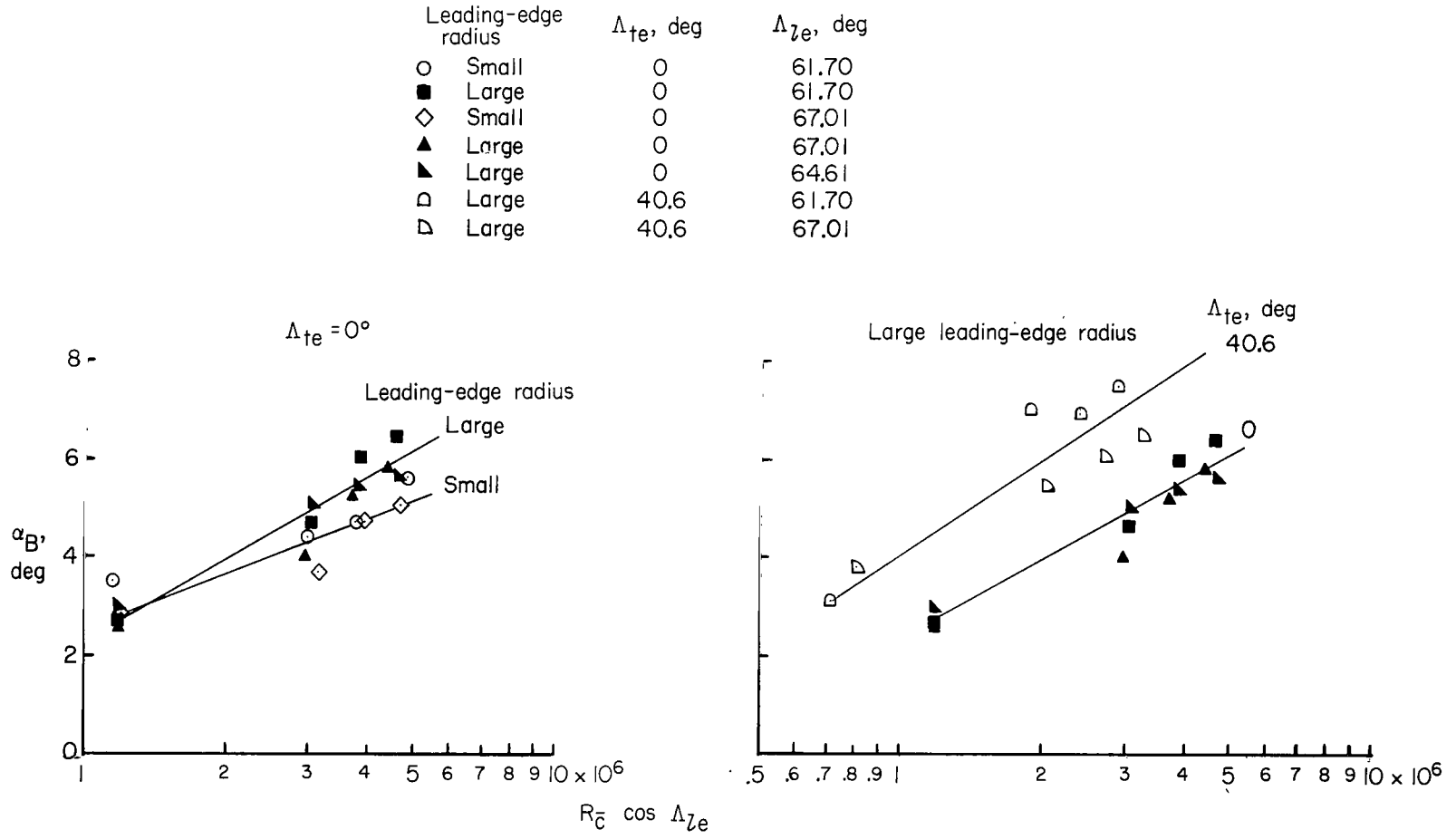


Figure 18.- Effect of leading-edge radius and trailing-edge sweep on variation of angle of attack at which leading-edge separation starts as function of Reynolds number.



015 001 C1 U A 770107 S00903DS  
DEPT OF THE AIR FORCE  
AF WEAPONS LABORATORY  
ATTN: TECHNICAL LIBRARY (SUL)  
KIRTLAND AFB NM 87117

POSTMASTER : If Undeliverable (Section 158  
Postal Manual) Do Not Return

*"The aeronautical and space activities of the United States shall be conducted so as to contribute . . . to the expansion of human knowledge of phenomena in the atmosphere and space. The Administration shall provide for the widest practicable and appropriate dissemination of information concerning its activities and the results thereof."*

—NATIONAL AERONAUTICS AND SPACE ACT OF 1958

## NASA SCIENTIFIC AND TECHNICAL PUBLICATIONS

**TECHNICAL REPORTS:** Scientific and technical information considered important, complete, and a lasting contribution to existing knowledge.

**TECHNICAL NOTES:** Information less broad in scope but nevertheless of importance as a contribution to existing knowledge.

**TECHNICAL MEMORANDUMS:** Information receiving limited distribution because of preliminary data, security classification, or other reasons. Also includes conference proceedings with either limited or unlimited distribution.

**CONTRACTOR REPORTS:** Scientific and technical information generated under a NASA contract or grant and considered an important contribution to existing knowledge.

**TECHNICAL TRANSLATIONS:** Information published in a foreign language considered to merit NASA distribution in English.

**SPECIAL PUBLICATIONS:** Information derived from or of value to NASA activities. Publications include final reports of major projects, monographs, data compilations, handbooks, sourcebooks, and special bibliographies.

**TECHNOLOGY UTILIZATION PUBLICATIONS:** Information on technology used by NASA that may be of particular interest in commercial and other non-aerospace applications. Publications include Tech Briefs, Technology Utilization Reports and Technology Surveys.

*Details on the availability of these publications may be obtained from:*

**SCIENTIFIC AND TECHNICAL INFORMATION OFFICE**  
**NATIONAL AERONAUTICS AND SPACE ADMINISTRATION**  
Washington, D.C. 20546